Synthesis, Biological Evaluation, and Crystallographic Studies of Extended Guanine-Based (*lin*-Benzoguanine) Inhibitors for tRNA-Guanine Transglycosylase (TGT)

by **Emmanuel A. Meyer**, **Nicola Donati**, **Marine Guillot**, **W. Bernd Schweizer**, and **François Diederich***

Laboratorium für Organische Chemie der Eidgenössischen Technischen Hochschule, ETH-Hönggerberg, HCI, CH-8093 Zürich (e-mail: diederich@org.chem.ethz.ch)

and

Bernhard Stengl, **Ruth Brenk**, **Klaus Reuter**, and **Gerhard Klebe***

Institut für Pharmazeutische Chemie der Philipps-Universität Marburg, Marbacher Weg 6, D-35032 Marburg

This paper describes the rational design, synthesis, and biological evaluation of a new generation of inhibitors of the bacterial enzyme tRNA-guanine transglycosylase (TGT), which has been identified as a new target in the fight against bacillary dysentery (Shigellosis). The enzyme catalyzes the exchange of guanine in the anticodon wobble position of tRNA by the modified base $preQ_1$, a guanine derivative, according to a ping-pong mechanism involving a covalent TGT-tRNA intermediate (*Fig. 2*). Based on computer modeling (*Fig. 3*), *lin*-benzoguanine (6-aminoimidazol[4,5-*g*]quinazolin-8(7*H*)-one (**2**)) was selected as an extended central scaffold, to form up to seven in-plane intermolecular H-bonds with the protein while sandwiching between Tyr106 and Met260. Versatile synthetic protocols were developed for the synthesis of **2**, and derivatives with phenyl, benzyl, and 2-phenylethyl side chains (*i.e.*, **16**, **17a**, and **12a**, **12b**, **13**, **17**, resp.) to reach into the lipophilic pocket lined by Val282, Val45, and Leu68 (*Schemes 1–3*). To account for the limited solubility of the new ligands and in consequence of a recently developed detailed understanding of the mechanism of TGT catalysis (*Fig. 2*), the enzyme kinetic assay was completely redesigned, providing competitive (K_{ic}) and uncompetitive (K_{iu}) inhibition constants with respect to tRNA binding by TGT. The modifications of the various parameters in the new assay are described in detail. Binding affinities of the new inhibitors were found to be in the single-digit micromolar range (K_{ic} values, *Fig. 8*). Decoration of the *lin*-benzoguanine scaffold with lipophilic residues only gave a modest improvement in biological activity which was explained on structural grounds with the help of four crystal structures (*Fig. 10*) obtained by soaking the protein with inhibitors **2** and **12a**–**12c**. Both biochemical and biostructural analyses reported in this paper provide a fertile basis for the development of more potent future generations of TGT inhibitors.

1. Introduction. – The bacterial enzyme tRNA-guanine transglycosylase (TGT) is involved in the infection pathway of *Shigella* species causing Shigellosis, a bacillary dysentery [1]. In the course of our investigations on structure-based drug design of TGT inhibitors, we recently described a new class of inhibitors based on the 2-aminoquinazolin-4(3*H*)-one scaffold **1a** (*Fig. 1*) [2–4].

In eubacteria, TGT is involved in the posttranslational modification of four specific tRNAs [5]. It catalyzes the exchange of guanine in the anticodon wobble position by the modified base $preQ_1$, a 7-deaza-7-aminomethyl derivative of guanine. Kinetic stud-

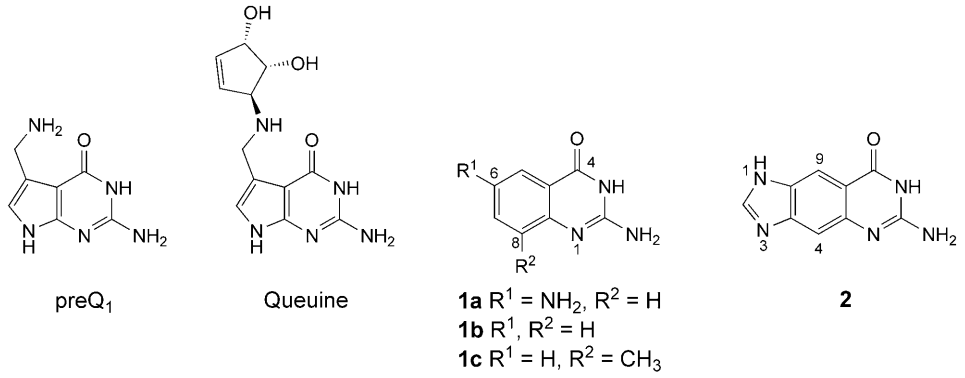

Fig. 1. *PreQ1* (natural substrate of eubacterial TGT) *and queuine* (end-product of biosynthetic pathway) *and synthetic TGT inhibitors* **1a**–**1c** *and* **2**

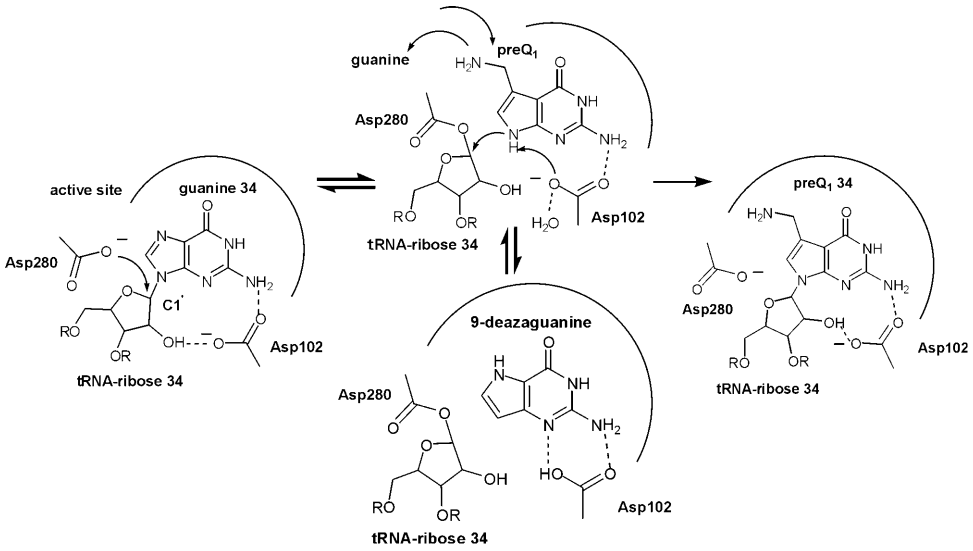

Fig. 2. *Schematic drawing of the base-exchange mechanism performed by TGT.* The exchange of guanine towards $preQ_1$ is performed in sequential steps *via* a covalent intermediate formed by Asp280. This intermediate state can be trapped by substrate analogs such as 9-deazaguanine.

ies clearly showed that the reaction pathway follows a ping-pong mechanism (*Fig. 2*) [6].

In a first step, unmodified tRNA binds with guanine in position 34 to the active site of TGT. In a second step, Asp280 undergoes nucleophilic attack at C(1′) of ribose 34, cleaving guanine from the tRNA strand. In the resulting intermediate state, tRNA is covalently bound to Asp280. Guanine is subsequently released from the binding pocket and replaced by the final substrate $preQ_1$. To activate $preQ_1$ for the nucleophilic attack on Asp280-C(1′), the base most presumably is deprotonated at position N(9) assisted by

Asp102 shuffling the proton from the active site *via* an adjacent H_2O molecule. $PreQ_1$ is then incorporated into tRNA resulting in product formation [7]. The structure of the covalent intermediate has recently been evidenced by crystal-structure analysis performed on a covalent TGT–tRNA intermediate [8]. A complex of TGT, covalently bound to tRNA, and the unreactive $preQ_1$-substrate analog 9-deazaguanine was trapped in the crystal after guanine had been released at the wobble position. The high relevance of this complex for the proposed enzyme mechanism is confirmed by the fact that, in the crystal, the non-reactive 9-deazaguanine can be replaced by $preQ_1$, resulting in the product, which exhibits $preQ_1$ covalently attached to tRNA. In subsequent steps, performed by other enzymes, the incorporated $preQ_1$ is further modified to queuine, one of the structurally most dramatically modified nucleobases found in nature [9]. Nucleoside modification is a common feature of tRNA [10], and up to 25% of the nucleosides show structural changes of the canonical bases [11]. However, the functional role of tRNA modification has yet to be elucidated. Most likely, it is related to structural stabilization or translational regulation of tRNA *via* its influence on codon–anticodon interactions. Variations in tRNA modification have been related to many human diseases, including cancer or infectious diseases [12]. In this context, *Durand et al.* showed that deletion of the gene encoding the tRNA-modifying enzyme TGT dramatically reduced the virulence of *Shigella*, the causative agent of bacillary dysentery (Shigellosis) [1]. Detailed crystallographic studies and biochemical characterization established TGT as a suitable enzymatic target for structure-based drug design. For these studies TGT from *Zymomonas mobilis* was used, as TGTs form *Shigella* are not suited for crystal structure analysis. Both TGTs are identical with respect to the active site besides one conservative exchange from phenylalanine 106 to tyrosine [13]. The selective inhibition of TGT could potentially lead to a new class of antibiotics based upon a unique mode of action. In the following, we present the design, synthesis, and *in vitro* evaluation of novel tricyclic TGT inhibitors based on the *lin*-benzoguanine scaffold **2**.

2. Results and Discussion. – 2.1. *Design of the Lead Structure.* Available space in the enzyme active site, as visualized through molecular modeling using the MOLOC software package [14], suggested us to use *lin*-benzoguanine **2** (trivial name for 6-aminoimidazol[4,5-*g*]quinazolin-8(7*H*)-one) as new lead scaffold for TGT inhibition (*Fig. 3*). Modified nucleobases such as **2** have been introduced nearly three decades ago by *Leonard* and co-workers [15][16] but have so far found only limited application as enzyme inhibitors [17]. In recent work by *Kool* and co-workers, extended adenine and thymidine derivatives were employed to construct a stable DNA double helix with expanded size [18].

Our new lead structure is characterized by the formal insertion of a benzene ring into the guanine heterocycle, which extends the lateral dimension of the scaffold by 2.4 Å. Compared to the natural substrate $preQ_1$ or 2-aminoquinazolin-4(3*H*)-one, the larger aromatic surface is expected to increase the stacking and *Van der Waals* interactions with Tyr106 and Met260, respectively, two residues forming the top and the bottom of the binding pocket. The scaffold should also retain the same H-bonding pattern as **1a** to Gly230, Gln203, and Asp156, residues involved in the specific recognition of guanine and $preQ_1$. The H-bond with the C=O of Leu231, seen in the recognition of

the aminomethyl group in preQ$_1$, is preserved by the presence of the imidazole NH in *lin*-benzoguanine.

Attachment of a *para*-substituted 2-phenylethyl side-chain would be envisaged at position 4 of the tricyclic scaffold, providing analogous spatial orientation of the lipophilic substituent in the apolar enzyme binding pocket as in the previous inhibitor generation [4].

2.2. *Synthesis of the Inhibitors.* Commercially available 1*H*-benzimidazole-6-carboxylic acid (**3**) was esterified to **4** (MeOH, $SOCl_2$) [19] and nitrated (fuming HNO_3, conc. H_2SO_4) in good yield (*Scheme 1*). To increase the solubility of benzimidazole **5** in organic solvents, and thus facilitate its purification, the imidazole moiety was protected by a benzyl group. The two regioisomers **6a** and **6b**, formed in nearly 1:1 ratio, were readily separated by column chromatography, and their identity was supported by NOE measurements, whereas correct assignment of the H–C(2,4,7) signals was achieved through ^{1}H,^{13}C-correlation spectroscopy. Further structural evidence was provided by the crystal structures of two following intermediates (see *Sect. 2.3*). Reduction of the NO_2 functionality with Zn in AcOH gave anthranilate **7a**, and subsequent iodination (I_2, $NaHCO_3$) provided the desired intermediate **8** in high yield.

Scheme 1. *Synthesis of Intermediate* **8** *and Lead Scaffold* **2**

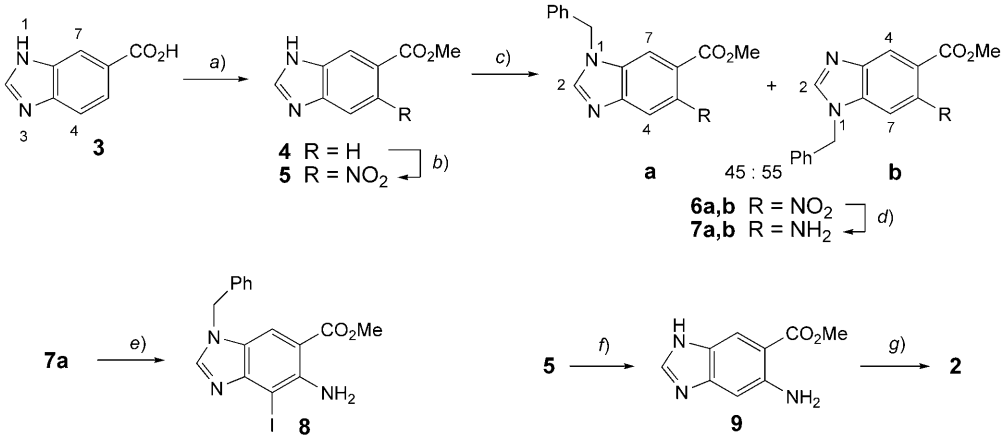

a) MeOH, $SOCl_2$, 50°; 96%. *b*) HNO_3, H_2SO_4, 50°; 68%. *c*) BnCl, NaH, Bu_4NI, THF, Δ; 93%. *d*) Zn, AcOH, H_2O, 20°; 85%. *e*) I_2, $NaHCO_3$, CH_2Cl_2, H_2O, 20°; 95%. *f*) H_2, Pd/C (10%), AcOH, Δ; 98%. *g*) Chloroformamidinium chloride, Me_2SO_2, 150°; 32%.

The unsubstituted lead structure **2** was obtained through reduction of **5** (H_2, Pd/C, AcOH), followed by cyclization of the resulting anthranilate **9** with chloroformamidinium chloride.

Sonogashira cross-coupling of **8** with three different alkynes, with $[PdCl_2(PPh_3)_2]$ as catalyst and CuI as co-catalyst in $(i\text{-Pr})_2NH$ provided the desired products **10a**–**10c** in good-to-excellent yield (*Scheme 2*) [20]. Hydrogenation (H_2, Pd/C) of the C≡C bond and concomitant deprotection of the benzimidazole moiety yielded **11a**–**11c**.

Interestingly, up to stoichiometric amounts of the Pd catalyst were required for completion of the two transformations. Finally, cyclization with chloroformamidinium

Scheme 2. *Synthesis of Inhibitors* **12a**–**12c**

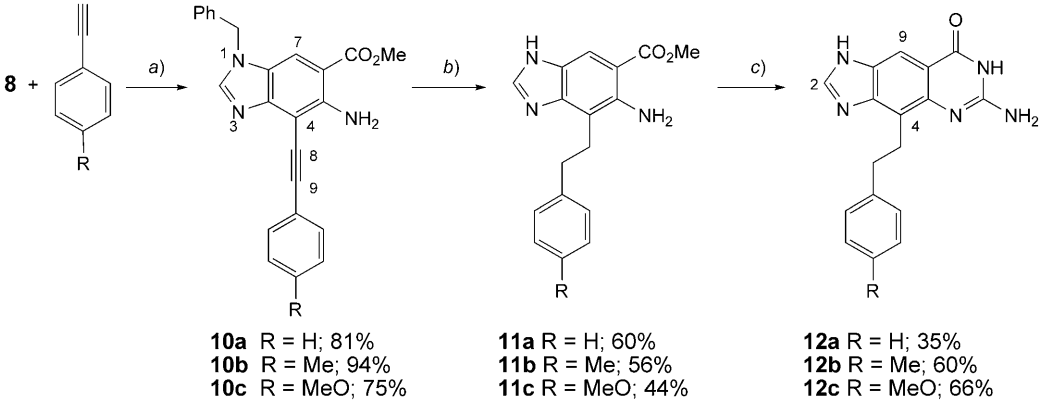

a) $[PdCl_2(PPh_3)_2]$, CuI, $(i\text{-Pr})_2NH$, 50°. *b*) H_2, Pd/C (10%), 20°. *c*) Chloroformamidinium chloride, Me_2SO_2, 150°.

chloride provided the desired inhibitors **12a**–**12c**. The tricyclic *lin*-benzoguanines showed tautomeric behavior, with respect to the NH position in the imidazole ring, in $(CD_3)_2SO$. The doubling of the ^{1}H-NMR signals for H–C(2) and H–C(9) could be eliminated by enhancing the rate of tautomerism through addition of few drops of D_2O and CF_3COOD (deuterated TFA). Full protonation of the compounds by TFA was required for the acquisition of highly resolved ^{13}C-NMR spectra. Tautomerism is influenced by a number of factors including concentration, temperature, solvent type, and pH (for a minireview, see [21]). Numerous theoretical and experimental studies have been devoted to the tautomerism of nucleobases, and guanine in particular [22–24], owing to the possible implication of tautomeric forms in the mispairing and subsequent replication errors of DNA [25]. Tautomeric equilibria in enzymatic pockets, although not well understood, can be shifted to higher-energy states through stabilization by H_2O molecules, binding residues with distinct local pH values, or metal cations [26]. In the case of TGT–benzoguanine complexation, the interaction of N(3)–H with the C=O group of Leu231 should provide significant stabilization of one tautomeric structure as shown in *Fig. 3*.

Two structural features are responsible for the observed poor water solubility of the new inhibitors **12a**–**12c**, which could be a major drawback for the development of *in vivo* tests: The aminopyrimidone moiety can undergo extensive H-bonding networks, and the extended flat π–surface of the *lin*-benzoguanines favors π–π stacking. Solubility is also very low in apolar solvents as a result of intermolecular H-bonding interactions, which can, however, be disrupted upon addition of dipolar aprotic solvents such as DMF or Me_2SO.

To increase the solubility, inhibitors were prepared lacking either the exocyclic NH_2 group in position 6, to reduce the H-bonding propensity, or featuring a Ph group orthogonal to the planar heterocycle, to prevent π–π interactions. Thus, the cyclization of **11a** with formamidinium acetate in EtOH afforded the desired inhibitor **13** without exocyclic NH_2 group (*Scheme 3*). Moreover, *Suzuki* cross-coupling of the iodinated

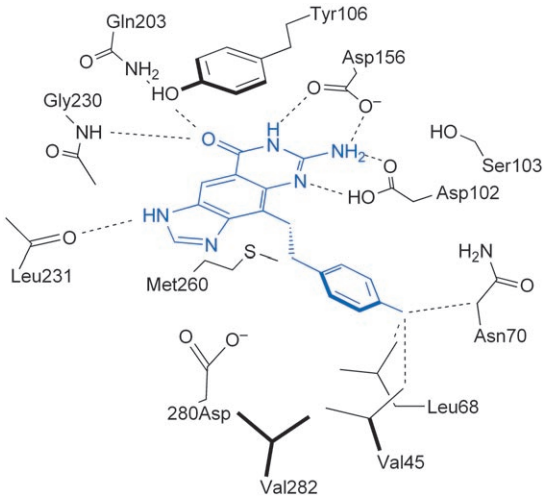

Fig. 3. *Schematic drawing of the binding mode of a* lin*-benzoguanine-based inhibitor into the active site of TGT.* The H-bonds and selected short apolar contacts are indicated as dotted lines.

Scheme 3. *Synthesis of Inhibitors* **13**, **16**, **17a**, *and* **17b**

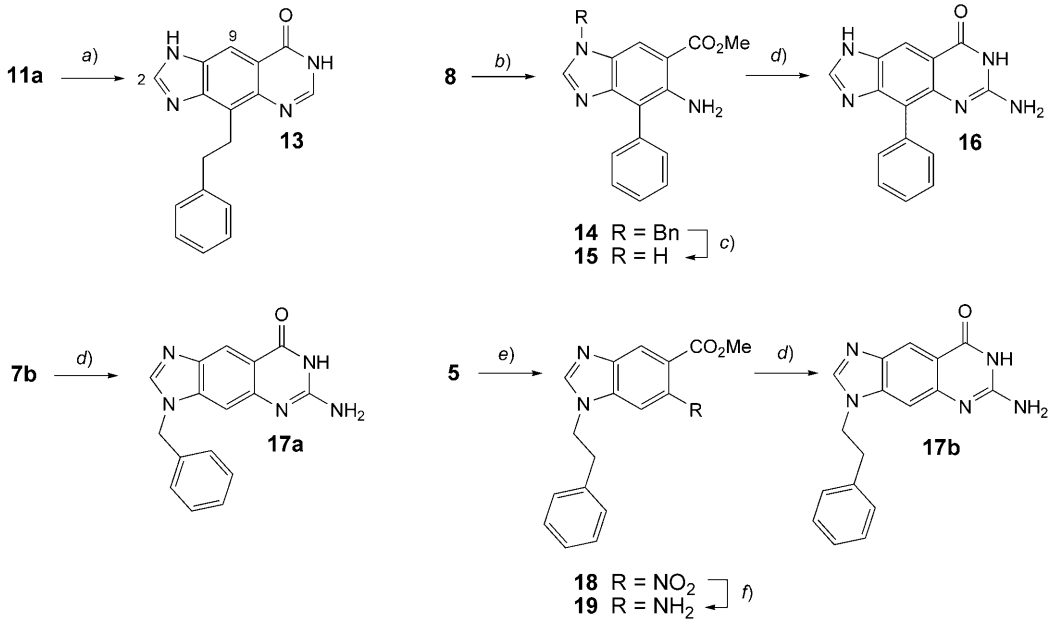

a) Formamidinium acetate, EtOH, 80°; 81%. *b*) Phenylboronic acid, $[Pd(PPh_3)_4]$, K_2CO_3, EtOH/H_2O/toluene, 80°; 87%. *c*) H_2, Pd/C (10%), EtOH, AcOH, 20°; 78%. *d*) Chloroformamidinium chloride, Me_2SO_2, 150°; 38–85%. *e*) $PhCH_2CH_2Cl$, NaH, THF, 80°, 12 h. *f*) H_2, Pd/C, AcOH, 20°, 12 h; 81%.

intermediate **8** with phenylboronic acid in a solvent mixture of toluene, EtOH, and H_2O gave 'biaryl-type' **14** in high yield (87%) [27].

Removal of the Bn group of **14** by hydrogenation and cyclization of the resulting anthranilate **15** furnished the desired inhibitor **16**. Gratifyingly, inhibitor **13** was soluble in hot MeOH, thus allowing purification by column chromatography (CH_2Cl_2/MeOH 95:5), whereas **16** showed no improvement in solubility in protic solvents and could only be dissolved in Me_2SO or DMF.

Two additional inhibitors, **17a** and **17b** with Bn or 2-phenylethyl side chains at the benzimidazole N-atom were prepared (*Scheme 3*). Thus, **17b** was obtained from **5** by alkylation with 2-phenylethyl chloride (→ **18**), reduction (→ **19**), and cyclization.

2.3. *Crystal Structures of Intermediates* **7b**, **8**, *and* **10b**. The constitution of **7b**, with the Bn group adjacent to C(7), was supported by X-ray crystal structure analysis (*Fig. 4*,*a*). Two conformers with different orientations of the Bn group are present in the unit cell forming two nested coils of H-bonded molecules (N(21)···O(18) 3.02/3.01 Å) around a 3_1 axis. The tautomeric structure of **8** was also confirmed by X-ray crystallography (*Fig. 4*,*b*). Also the position of the NH_2 group suggests intermolecular N–H/π interactions [28] between a pair of molecules **8** (N-centroid distance: 3.25 Å). One of the H-atoms forms an intramolecular H-bond with O(19) and the second H-atom points to C(15) of the Ph ring. Furthermore, the crystal packing features an edge-to-face aromatic interaction with a centroid-to-centroid distance of 4.96 Å. The crystal structure of compound **10b** revealed a nearly perfect planar alignment of the central core and the phenylethynyl moiety (*Fig. 4*,*c*). It is noticeable that the lowest-energy conformation of tolane in the gas phase features an orthogonal alignment of the two aromatic rings [29]. In the crystal lattice of **10b**, dimers are formed with a O(20)···N(21) interaction (shared with an intramolecular N(21)···O(20) H-bond) through a centre of symmetry that arrange with the next layer to show an antiparallel dipolar alignment of two C=O groups (distance between the two antiparallel C=O bonds: 3.56 Å).

2.4. *Biological Activity and Crystallographic Studies.* All newly synthesized inhibitors were tested for their inhibitory potency against TGT (*Z. mobilis*). Furthermore, we succeeded to determine the crystal structures of four inhibitors presented in this contribution in complex with *Z. mobilis* TGT.

2.4.1. *Adapted Kinetic Assay.* Faced by the problem of low solubility of some of our ligands and in consequence of a more-detailed understanding of the base exchange mechanism involving competitive and non-competitive inhibition, we had to redesign our enzyme kinetic assay. To appreciate these findings, several parameters of the previously applied assay were modified [13]. In the following, we present the motivation for each modification and its implications on the assay design.

2.4.1.1. *Ligand Solubility.* Some of our compounds exhibit low solubility under the applied assay conditions. Effects of low solubility can be manifold. As a consequence of possible precipitation, the resulting inhibition constants could be underestimated. However, also the opposite could be observed. As recently reported, the risk of unspecific inhibition exists for a large variety of compounds in particular if low solubility is given. Such behavior has been referred to as 'promiscuous inhibition' [30]. These compounds show up repeatedly as inhibitors of various enzymes in biological assays. However, they do not follow a target-specific mode of action. Instead, such behavior is

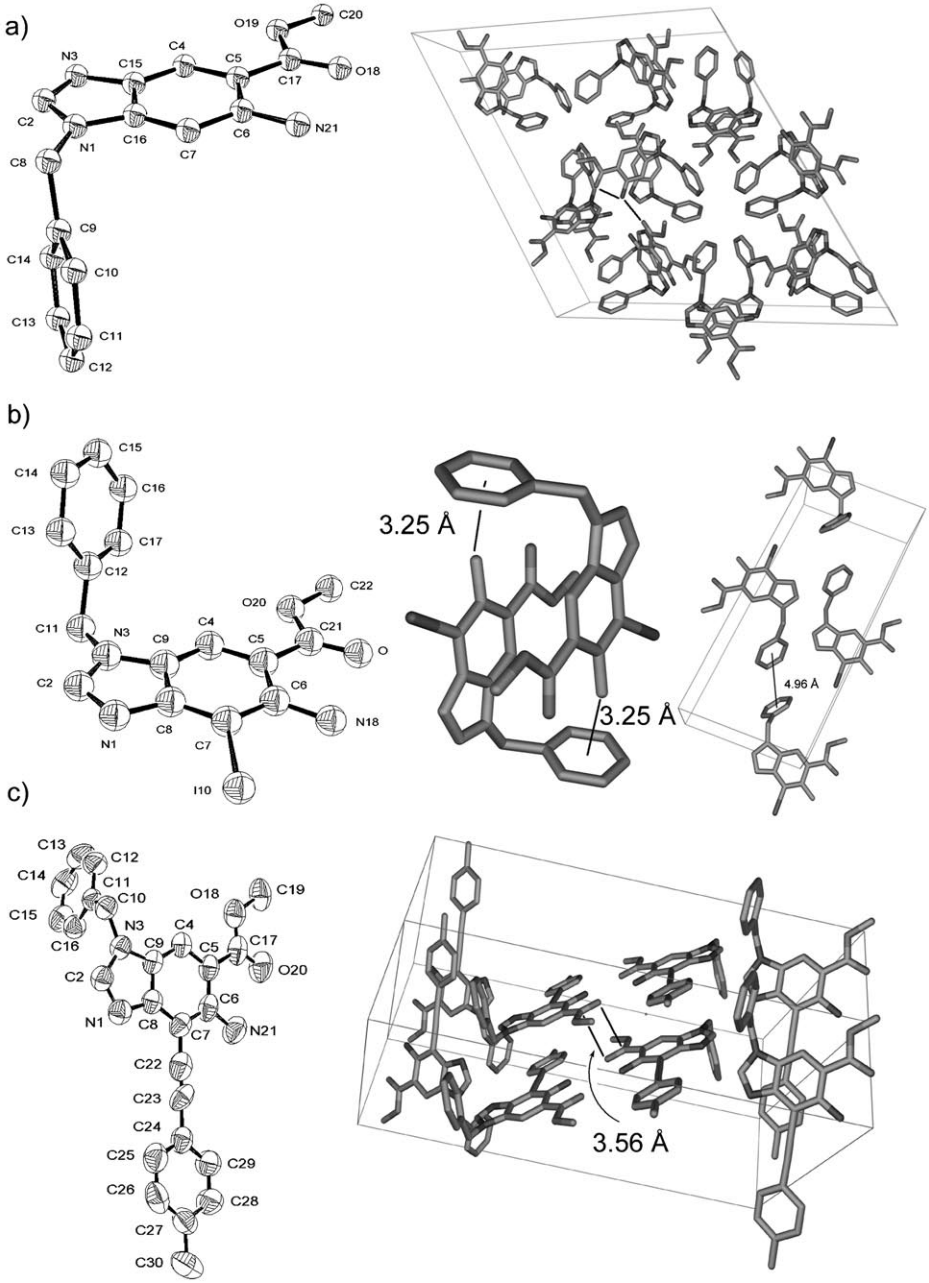

Fig. 4. a) *X-Ray crystal structure of* **7b** (left) *with unit cell* (right). b) *X-Ray crystal structure of* **8** (left) *with the N–H/π interactions* (middle), *and the unit cell* (right). c) *X-Ray crystal structure of* **10b** (left) *with the unit cell* (right). Arbitrary numbering. Atomic displacement parameters in the ORTEP plots obtained at 293 K are drawn at the 50% probability level.

thought to result from some sort of compound agglomeration that adsorbs the enzyme onto its aggregated surface. In consequence, the enzyme is inactivated. Adding detergents such as *Tween 20* or *Triton X-100* to the respective assay solutions obviously reduces aggregate formation and thus allows to distinguish 'promiscuous' from specific inhibitors [31]. To avoid possible effects of 'promiscuous inhibition' or other undesired precipitation effects in the aqueous TGT assay, *Tween 20* was added in 5% of its critical micellar concentration (CMC) of 59 μM. The amount of *Tween 20* used is based on the results reported by *Ryan et al.* [31].

2.4.1.2. *TGT Solubility and Kinetic Parameters.* As a supplementary effect, the use of detergents influences not only ligand but also protein solubility [31]. In particular *Tween 20* was described to reduce protein absorption onto plastic surfaces of cups usually used for kinetic measurements. Such artificial immobilization results in a reduced effective enzyme concentration in the assay solution [31]. Therefore, we reexamined the kinetic parameters for TGT to quantify the possible impact of *Tween 20*. Furthermore, accurately determined kinetic parameters are required to derive inhibition constants. K_m Values for TGT with respect to both substrates $tRNA^{Tyr}$ and [8-^{3}H]guanine (*Table*) remain within the range already published for *Z. mobilis* TGT ($K_m(tRNA^{Tyr})$: 0.2–1.0 μM; K_m([8-^{3}H]guanine): 0.38–1.3 μM) [32][33]. ^{3}H-Labeled guanine was used as alternative substrate instead of natural $preQ_1$, for which no labeled material was available.

Table. *Kinetic Characterization of Wild Type TGT with $tRNA^{Tyr}$ and [8-^{3}H]Guanine as Substrate in Presence of* Tween 20 ($c = 5\%$ CMC)

Parameter	[^{3}H]guanine		$tRNA^{Tyr}$	
	New values	Previous values[a])	New values	Previous values[a])
K_m [μM]	1.2 ± 0.2	0.38	0.9 ± 0.2	1.0
k_{cat} [s^{-1}]	$2.8 \cdot 10^{-2} \pm 0.1 \cdot 10^{-2}$	$1.1 \cdot 10^{-2}$	$2.7 \cdot 10^{-2} \pm 0.1 \cdot 10^{-2}$	$1.4 \cdot 10^{-2}$
k_{cat}/K_m [$\mu M^{-1}\ s^{-1}$]	$2.3 \cdot 10^{-2} \pm 0.6 \cdot 10^{-2}$	$2.9 \cdot 10^{-2}$	$3.0 \cdot 10^{-2} \pm 0.7 \cdot 10^{-2}$	$1.4 \cdot 10^{-2}$

[a]) Previous values as reported in [33].

In contrast, k_{cat} values significantly higher than those reported in [33] are obtained. Most likely, this observation results from a higher effective TGT concentration in the *Tween 20*-containing assay solution. Accordingly, we assume that the principal catalytic properties are not affected by added *Tween 20*.

2.4.1.3. *Preincubation of TGT with Inhibitor.* Pre-incubation of *Z. mobilis* TGT with a putative inhibitor was reported to affect the initial velocity of the enzyme-catalyzed reaction [33]. A 10-min pre-incubation of TGT with the inhibitor to be tested prior to the addition of substrate showed reduced initial velocity by *ca.* 50%. In contrast to this finding, the addition of *Tween 20* ($c = 5\%$ CMC) rather resulted in a slight increase of the initial velocity after a 10-min pre-incubation. Compared to tests in the absence of *Tween 20*, the initial velocity after 10-min preincubation increased by a factor of three. We assume that the previously observed pre-incubation effect resulted from a superimposed slow adsorption/desorption process of the enzyme from the plastic cups, which is unmasked by the use of *Tween 20*.

2.4.1.4. *Competitive and Uncompetitive Inhibition.* Recent kinetic and crystallographic studies provide a better insight into the molecular details of the TGT base-exchange reaction [6][8]. Competitive and uncompetitive inhibition of the binding of tRNA as substrate have to be considered with respect to the stepwise enzyme reaction, as already assumed in [4]. Due to these considerations, the originally applied assay protocol to determine inhibition constants (K_i) had to be altered.

The TGT-catalyzed reaction involves two substrates, tRNA and [8-^{3}H]guanine. For each, TGT provides a distinct binding pocket partially formed upon substrate binding. While tRNA interacts with apo TGT, [8-^{3}H]guanine binds in a subsequent step into a modified binding pocket partially formed by the covalently bound tRNA. The crystal structure of the 'ternary' TGT-tRNA·9-deazaguanine complex suggests that compounds of similar size such as the competitive substrate mimic 9-deazaguanine can be accommodated in this binding pocket *via* non-covalent interactions (*Fig. 2*). Accordingly, this site can either accommodate active substrates (*e.g.*, guanine or preQ$_1$) or other small ligands such as 9-deazaguanine. In the series of our studied inhibitors, some compounds exhibit molecular dimensions similar to the natural substrates, in particular our lead structures **1a** and **1b**, and **2**. Once decorated by additional aliphatic substituents, as in **12a**–**12c** or **16**, steric clashes with the covalently bound tRNA ribose moiety at position 34 can be expected. Accordingly, it can be assumed that these extended compounds compete only with tRNA binding to uncomplexed TGT (*Fig. 5*).

To verify this assumption, a trapping experiment, based on the covalent TGT–RNA intermediate was performed, similar to the study of *Xie et al.*, using 9-deazaguanine [8]. In different reaction mixtures, TGT was first incubated with an excess of tRNA

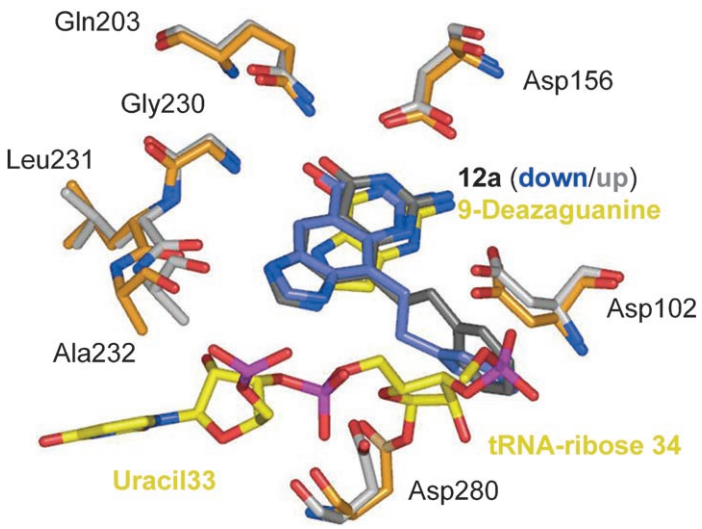

Fig. 5. *Superimposition of TGT crystal structures in complex with tRNA and inhibitor* **12a**. Shown in orange/yellow colors is the TGT active site in complex with 9-deazaguanine and tRNA covalently bound to Asp280. Shown in grey/blue colors is TGT in complex with **12a** in two alternative conformations. The 2-phenylethyl substituent of **12a** clearly interferes with the tRNA binding site. Color coding: N: blue, O: red, P: purple.

together with various inhibitors, *i.e.*, **1a**, **1b**, **2**, **12a**–**12c**. Then, an SDS-PAGE analysis of these mixtures was performed (*Fig. 6*). Bands are observed for uncomplexed TGT at 43.5 kDa (*Fig. 6*, *Lane 2*). Incubation of TGT with tRNA results in two additional, faint, retarded bands at about 70 kDa (*Fig. 6*, *Lane 3*). These bands correspond to covalent TGT–tRNA complexes [34]. The detection of two bands for the covalent complex results from different tRNA conformers present under the applied PAGE conditions as already reported in [35]. The occurrence of well-defined bands for TGT–tRNA in the presence of small inhibitors such as **1a**, **1b**, and **2** (*Fig. 6*, *Lanes 7–9*) clearly indicates the power of these ligands to stabilize the covalent intermediate similarly to 9-deazaguanine [8]. Once exposed to inhibitors exhibiting a large substituent at their basic scaffolds such as **12a**–**12c** (*Fig. 6*, *Lanes 4–6*), the respective bands are only very faint, similar to the situation when pure TGT is mixed with tRNA in absence of a small molecule inhibitor (*Fig. 6*, *Lane 3*). This finding indicates that inhibitors of the size of **12a**–**12c** are not capable to stabilize the TGT–tRNA complex.

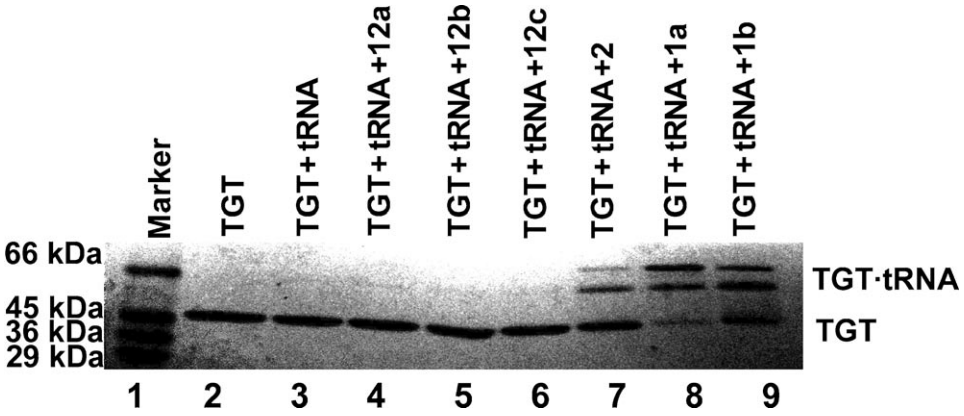

Fig. 6. *SDS-PAGE Analysis of trapping experiments performed with TGT/tRNA mixtures together with inhibitors of different size.* While small inhibitors, **1a**, **1b**, and **2** cause retarded TGT bands by stabilizing the covalent TGT-tRNA intermediate, functionalized, more extended inhibitors, **12a**–**12c**, lack this ability. The covalent band is as faint as in pure TGT/tRNA mixtures. SDS-7 Marker (mixture of proteins with different sizes) was used to estimate molecular weight.

In consequence, we assume that size-dependent inhibition models with respect to tRNA and [^{3}H]guanine as limiting substrates have to be considered in the K_i determination. Inhibitors with large side chains are expected to be competitive only with tRNA, binding to TGT as substrate. Small inhibitors of comparable size to the natural nucleobase substrates exhibit a more complex inhibition potency. They either occupy the base-exchange site prior to tRNA binding to TGT, a step which is, to some extent, competitive with tRNA binding. That such kind of binding is possible can be concluded from the formation of binary TGT·inhibitor complexes seen in many crystal structures [3][4]. Alternatively, they compete with preQ$_1$ or guanine after tRNA is covalently attached to TGT. Accordingly, to compare small guanine-sized and larger, extended inhibitors, their binding constants determined with respect to tRNA binding are required to provide directly comparable inhibitory values. In our previously applied

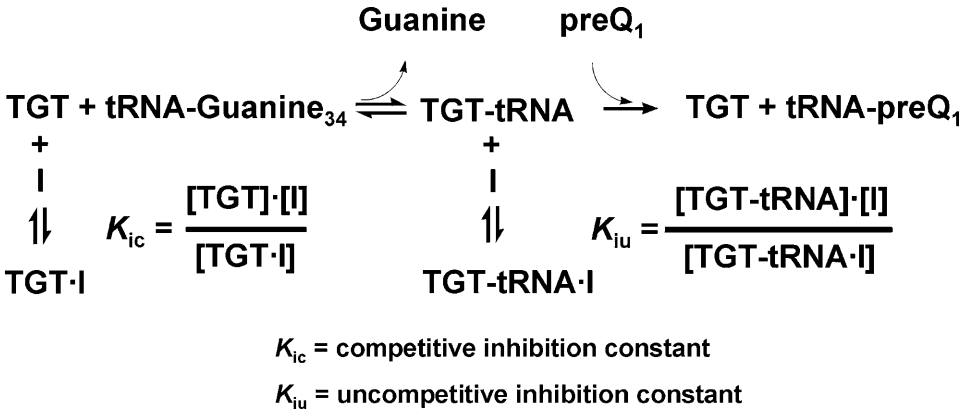

Fig. 7. *Inhibition of TGT with respect to tRNA binding, resulting in competitive and uncompetitive inhibition constants*

assay protocol, inhibition constants were determined with respect to [8-^{3}H]guanine as limiting substrate. In the new protocol [8-^{3}H]guanine is used in 20 μM excess, while the $tRNA^{Tyr}$ concentration is now limiting.

Nevertheless, for inhibitors of the guanine-type size two inhibition constants have to be defined that fully characterize their TGT inhibition with respect to tRNA binding (*Fig. 7*).

Small inhibitors such as **1a**, **1b**, and **2** might act as competitive inhibitors with respect to tRNA binding (K_{ic}), occupying the base-recognition site of TGT prior to tRNA binding. If their binding occurs subsequently to tRNA binding, and after cleavage and release of the natural substrate guanine from the base-recognition site, stabilization of the covalent TGT–tRNA adduct will be the result. In this case they act as uncompetitive inhibitors with respect to tRNA binding (K_{iu}). Such a competitive/uncompetitive inhibition process can be described by a double reciprocal *Lineweaver–Burk* plot according to *Eqn. 1*. This relationship exhibits two inhibition constants, K_{ic} and K_{iu}. While competitive inhibition results in a raise of K_m, uncompetitive inhibition decelerates V_{max}. Both inhibition constants contribute to the total inhibition of TGT with respect to tRNA binding, and both have to be considered to determine the amount of compound needed to suppress the readout of the assay, namely the incorporation of [8-^{3}H]guanine in tRNA replacing unlabeled guanine. In the literature, such a composite type of inhibition is referred to as mixed or non-competitive inhibition [36][37].

$$\frac{1}{v_0} = \left[\frac{K_m}{V_{max}} \cdot \left(1 + \frac{[I]}{K_{ic}}\right)\right] \cdot \frac{1}{[S]} + \frac{1}{V_{max}} \cdot \left(1 + \frac{[I]}{K_{iu}}\right) \quad (1)$$

For inhibitors with a large side chain such as **12a**–**12c** and **16**, the competitive inhibition constant K_{ic} is supposedly sufficient to fully describe their inhibition properties, as these compounds are too large to be significantly accommodated by the binding pocket

as long as the covalent TGT–tRNA adduct is formed. K_{iu} is hardly relevant in this case, and the respective inhibition type can be described as predominantly competitive. *Eqn. 2* describing the latter situation results from a simplification of *Eqn. 1*. The competitive inhibition constant K_{ic} either for guanine-sized or substituted inhibitors describes in both cases the potential to impede tRNA binding to TGT. Thus, the K_{ic} values for both types of inhibitors are directly comparable.

$$\frac{1}{v_0} = \left[\frac{K_m}{V_{max}} \cdot \left(1 + \frac{[I]}{K_{ic}}\right)\right] \cdot \frac{1}{[S]} + \frac{1}{V_{max}} \tag{2}$$

The modified assay conditions take impact on the resulting inhibition constants. Therefore, it is difficult to directly link our previously reported inhibition constants to the re-evaluated ones presented in this study. In particular the replacement of [8-^{3}H]guanine by tRNA as limiting substrate, the appropriate consideration of a superimposed uncompetitive inhibition mode, and the addition of a detergent to enhance solubility modulates the inhibition constants to some, however, across the entire data set not linear fashion. Accordingly, re-evaluation of the most relevant compounds, reported earlier, appeared essential.

2.4.2. *Inhibition Constants.* Inhibition constants for *lin*-benzoguanine **2** and some *N*- and 4-substituted derivatives, **12a**–**12c**, **13**, **16**, **17a** and **17b**, are given in *Fig. 8*. As ligand **2** was identified as competitive/uncompetitive inhibitor, we also decided to re-evaluate several of the small, guanine-size inhibitors, **1a**–**1d**.

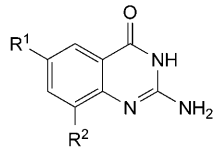

1a $R^1 = NH_2$, $R^2 = H$ K_{ic} = 1.5 μM; K_{iu} = 0.6 μM
1b R^1, $R^2 = H$ K_{ic} = 2.1 μM; K_{iu} = 1.7 μM
1c $R^1 = H$, $R^2 = Me$ K_{ic} = 3.7 μM; K_{iu} = 19.1 μM

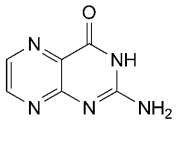

1d K_{ic} = 2.2 μM; K_{iu} = 0.7 μM

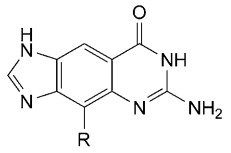

2 R = H K_{ic} = 4.1 μM; K_{iu} = 7.9 μM
16 R = Ph K_{ic} = 29 ± 7 μM

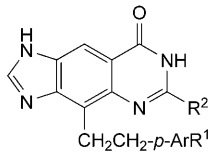

12a $R^1 = H$, $R^2 = NH_2$ K_{ic} = 1.0 ± 0.3 μM; K_{iu} = 40 – 70 μM
12b $R^1 = Me$, $R^2 = NH_2$ K_{ic} = 6.9 ± 1.7 μM
12c $R^1 = MeO$, $R^2 = NH_2$ K_{ic} = 3.7 ± 0.9 μM
13 $R^1 = H$, $R^2 = H$ K_{ic} = 2.8 ± 0.7 μM

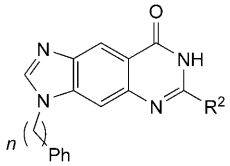

17a *n* = 1 K_{ic} = 15 μM
17b *n* = 2 K_{ic} = 7.3 μM

Fig. 8. *Biological activities* (K_{ic} and K_{iu} values) *of quinazolinone-, pteridine-, and* lin-*benzoguanine-based inhibitors*

Ligands **1a** and **1b** were identified by the trapping experiment as uncompetitive inhibitors (*Sect. 2.4.1.4*). Their K_{iu} constants indicate decreasing power to stabilize the covalent adduct from **1a** (0.6 μM), over **1b** (1.7 μM), to **2** (7.9 μM). This descending order is also reflected by the intensities of the bands at 70 kDa (*Fig. 6*, *Lanes 7–9*). Facing the competitive inhibition constants (K_{ic}) also shows a slightly reduced potency of **2** (4.1 μM) compared to **1a** (1.5 μM) and **1b** (2.1 μM). Our previously reported, too-low inhibition constant of **1b** (20–50 nM) results from the neglect of the uncompetitive inhibition in the old assay [4]. Therefore, in particular the small guanine-type inhibitors have been overestimated with respect to their inhibition power. To verify these observations, the natural compound pteridine **1d**, previously described as potent inhibitor in the higher nanomolar range [38], was also tested for mixed inhibition. With a K_{ic} value of 2.2 μM, it is a competitive inhibitor in a similar activity range to **1b**, while its uncompetitive inhibition of 0.7 μM is in the range of that of **1a**.

Ligand **1c**, a Me-substituted derivative of **1b** also shows competitive/uncompetitive inhibition, although the competitive contribution dominates (K_{ic} = 3.7 μM *vs.* K_{iu} = 19.1 μM). Consistently, the 70-kDa covalent bands in the respective trapping experiment are less pronounced than for **2** (data not shown). In structural terms, this observation can be explained by spatial conflicts, with the attached Me group in **1c** most likely interfering with the ribose ring 34 of the covalently bound tRNA. This effect is even more pronounced for inhibitors bearing larger side chains at this position.

Compounds **12a**–**12c**, **13**, **16**, **17a**, and **17b** almost purely act as competitive inhibitors. In the trapping experiment, only faint covalent bands remained detectable (*Fig. 6*; data shown only for **12a**–**12c**). Ligand **12a** exhibits the lowest K_{ic} value (1.0 μM) in the studied series (*Fig. 8*), resulting in a modest enhancement over **2** by a factor of 4. However, a weak uncompetitive contribution of **12a** (K_{iu} = 40–70 μM) could be determined as well. The value of K_{iu} is separated from K_{ic} by almost two orders of magnitude. Thus, it does not contribute significantly to the total inhibition. Nevertheless, obviously binding of **12a** is still possible once tRNA is covalently attached to TGT (*cf. Fig. 5*). Supposedly, the **12a** side chain adopts a conformation that allows for its non-repulsive placement next to the bound tRNA. In consequence, a marginal uncompetitive contribution to inhibition, undetectable by trapping experiments, cannot be excluded also for other substituted inhibitors. As it was not feasible to determine K_{iu} for all substituted inhibitors, this presumably marginal contribution, indicated by the trapping experiments, has been neglected in the kinetic measurements. Only K_{ic} values have been determined for these compounds.

Compound **13** lacks the C(6)–NH_2 group compared to ligand **12a**. Its loss in affinity demonstrates the importance of this functionality for binding (**13** *vs.* **12a**: K_{ic} 2.8 μM *vs.* 1.0 μM) mediating polar interactions to Asp156 and Asp102 (see *Fig. 3*). Additional substitution of the Ph ring in compound **12a** with a *p*-Me (**12b**; K_{ic} 6.9 μM) or a *p*-MeO group (**12c**; K_{ic} 3.7 μM) appears detrimental to binding. Immediate attachment of the Ph group in **16** results in a substantial loss in activity (K_{ic} 29 μM). Similarly, the *N(3)*-substituted benzoguanines experience a loss in affinity (**17a**, 15.4 μM; **17b**, 7.3 μM).

Fig. 9 shows the inhibition constants for previously described inhibitors measured under our new assay conditions [2][4]. All compounds were identified to be primarily competitive inhibitors *via* trapping experiments. Competitive inhibition constants (K_{ic}) for most phenyl-substituted quinazolinones were determined to be in the single-digit

μM range. The large difference in binding affinity between S-, O-, and C-atoms in the linker is no longer observed. Compounds with substituents other than unsubstituted Ph rings show reduced affinity.

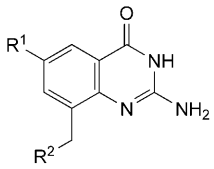

R^1 = NH_2, R^2 = $PhCH_2$	K_{ic} = 2.6 μM	R^1 = CN, R^2 = PhS	K_{ic} = 6.4 μM
R^1 = NH_2, R^2 = PhO	K_{ic} = 5.7 μM	R^1 = H_2NCH_2, R^2 = PhS	K_{ic} = 16 μM
R^1 = NH_2, R^2 = PhS	K_{ic} = 3.8 μM	R^1 = NH_2, R^2 = PrS	K_{ic} = 14 μM
R^1 = H, R^2 = PhS	K_{ic} = 4.0 μM	R^1 = NH_2, R^2 = imidazol-2-yl-S	K_{ic} = 34 μM
R^1 = OH, R^2 = PhO	K_{ic} = 8.7 μM	R^1 = NH_2, R^2 = $Me_2N(CH_2)_2$-S	K_{ic} = 22 μM
R^1 = OH, R^2 = PhS	K_{ic} = 5.1 μM	R^1 = NH_2, R^2 = 3-BrPhS	K_{ic} = 24 μM

Fig. 9. *Biological activities* (K_{ic} values) *of quinazolinone-based inhibitors* (from [4][28])

2.4.3. *Crystal-Structure Analysis.* Some of the newly synthesized inhibitors were crystallized as binary complexes with TGT. Although quite low (see *Sect. 2.4.1.1*), the solubility of the *lin*-benzoguanine-based inhibitors is superior to that of the quinazolinone-based ligands presented in [3][4], which allowed the application of soaking methods. Thus, crystals with unsubstituted **2** and **12a**–**12c** could be obtained, whereas reduced solubility of **16**, **17a**, and **17b** impeded similar attempts. Details on the crystal structure analyses will be given in [39]. *Fig. 10*, *a* shows how the core scaffold **2** is involved in an H-bonding pattern, as expected from modeling (*Fig. 3*). With respect to structures of uncomplexed TGT, Asn70 adopts a shifted conformation, thus inducing a slightly altered binding pocket. Ligand **12a** adopts in the crystal two different, almost equally populated conformations. The 2-phenylethyl substituent is oriented either above (up-conformation) or below (down-conformation) a best plane through the tricyclic ring system, respectively. In the up-conformation, the adjacent Asn70 is oriented similarly as in the complex with **2**. In contrast, in the down-conformation, Asn70 resides in a geometry similar to uncomplexed TGT (conformational change indicated by arrow in *Fig. 10*, *b*). In ligand **12b**, the side chain is nearly exclusively found with limited accuracy in the up-conformation (*Fig. 10*, *c*), while Asn70 occurs equally populated in both already mentioned conformations. Possibly the down-conformation for the ligand side chain is hardly adopted due to repulsive contacts of the *p*-Me group with Asn70 in either of its two orientations. Finally, **12c** with a *p*-MeO group occurs in only one conformation with respect to both side chain and Asn70 (*Fig. 10*, *d*). Surprisingly, in this case, the side chain adopts the down-conformation; however, with limited accuracy for the side chain as well as for the scaffold electron density. Asn70 is found in a geometry similar to uncomplexed TGT. The latter three structures point to substantial conformational adaptations of the TGT binding pocket next to Asn70 upon ligand binding. Depending on the conformational properties of the side chain and its steric demand, conformational disorder is observed to varying extent.

The crystal structures provide an explanation for the only marginal gain in inhibition power upon decoration of the central scaffold with a substituted 2-phenylethyl side chain (*e.g.*, **12a**–**12c** compared to parent scaffold **2**). Despite significant gain in lipophilic surface, K_{ic} values do not improve tremendously. The particular positioning of the 1,2-ethanediyl linkers in **12a**–**12c**, connecting the parent scaffold with the phenyl moiety, provides a possible explanation for this observation. They protrude into the highly polar solvation spheres of Asp280, the catalytic nucleophile, and Asp102,

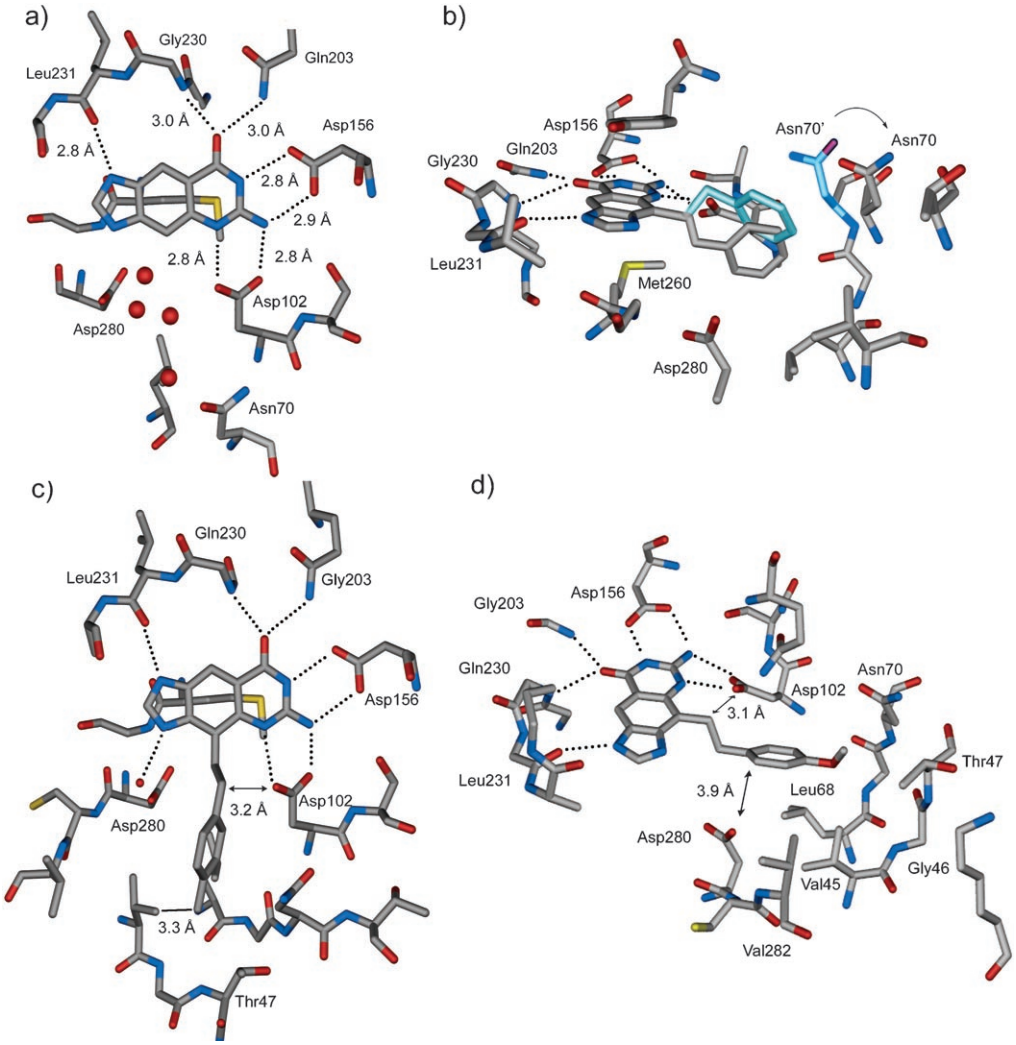

Fig. 10. *Four different crystal structures of TGT–inhibitor complexes.* All complexes were obtained by soaking TGT crystals with a solution of the inhibitor at pH 5.5; dotted lines: H-bonds. TGT is complexed to: *a*) **2**, red spheres are isolated bound H_2O molecules; 1.7 Å resolution. *b*) **12a**, 1.58-Å Resolution; light blue residue: alternative up-conformation of **12a** with induced conformational change at Asn70. *c*) **12b**, 1.58-Å Resolution; arrow: unfavorable intermolecular contact. *d*) **12c**, 2.1-Å Resolution. Color coding: N: blue, O: red, S: yellow, C: grey.

involved in deprotonation of the substrate base. Thus, unfavorable proximities between a CH_2 moiety of the linker and a side chain O-atom of Asp102 are clearly visible in the complex of **12b** (d(C···O) 3.2 Å) and **12c** (d(C···O) 3.1 Å.) Presumably, this penetration is detrimental to binding affinity. If this area remains unoccupied, such as with bound **2**, these polar residues are involved in a subtle crystal H_2O network (*Fig. 10*,*a*). Supposedly, any rupture of this solvation network reduces affinity. This loss is

also reflected by the higher K_{ic} value of **1c** (3.7 μM) compared to **1b** (2.1 μM). Crystal-structure analyses of both compounds complexed with TGT also indicated repulsive interactions of the Me group in **1c** with Asp102 and the neighboring H_2O molecules [4]. Due to these unfavorable interactions, we assume that **12a**–**12c** suffer significant affinity loss, which is only partially compensated by the additional hydrophobic interactions experienced in the newly created lipophilic subpocket next to Asn70, lined by the side chains of Val282, Val45, and Leu68. Across the series, **12a** seems to better match the lipophilic pocket than **12b** and **12c**, resulting in a better defined electron density for the side chain. This provides also a structural explanation for the lower K_{ic} value of **12a**.

3. Conclusions. – In this study on the rational development of tRNA-guanine transglycosylase (TGT) inhibitors, we reported the introduction of a new scaffold based on *lin*-benzoguanine **2**. Versatile synthetic protocols were developed (*Schemes 1–3*), and binding affinity (competitive inhibition constants K_{ic} with respect to tRNA binding) in the single-digit μM range could be achieved (*Fig. 8*). The crystallographic studies demonstrated a ligand-induced widening at Asn70 of the apolar distal binding pocket lined by the side chains of Val282, Val45, and Leu68 (*Fig. 10*). The crystal structures show unfavorable contacts between the 2-phenylethyl side chains of inhibitors **12a**–**12c** and the carboxylate of Asp102, presumably responsible for the only moderate binding affinity enhancement of these ligands with respect to the lead scaffold **2**. In previous medicinal chemistry-related projects from this laboratory, modeling was performed based upon different levels of flexibility of the binding pocket, ranging from rigid in the case of thrombin to highly flexible in plasmepsin II, in which the flap pocket undergoes major conformational changes (for a short review, see [40]). Our studies on TGT emphasize its moderate plasticity, with a flip of the peptidic backbone at Leu231/Ala232 and a rotation of Asp102 as described in [4][33], and ligand-induced conformational changes at Asn70, as observed in this study. During the design cycle, our understanding of TGT evolved, therefore, from a rigid to a fairly flexible enzymatic pocket, wherein subtle variations in inhibitor structure were responsible for critical changes in activity. From a biosynthetic point of view, moderate conformational flexibility of TGT is needed to perform the complex transglycosylation reaction on specific tRNAs without external energy sources (co-factors) and to achieve the functionally required substrate promiscuity.

The presence of tRNA in the binding assay complicates, however, the interpretation of biological data. Thus, band-shift experiments suggest different mode of action for our designed inhibitors (*Fig. 6*). Whereas all inhibitors, including side-chain-bearing ligands such as **12a**–**12c**, act as competitive inhibitors with respect to tRNA, only small inhibitors such as **1a**, **1b**, or **2** additionally stabilize the covalent tRNA–TGT intermediate in a 'ternary' complex. The structural information gained in this work provides fertile ground for further development of TGT inhibitors.

We are grateful to the *ETH Research Council* and the *Fonds der Chemischen Industrie* for support of the work done at the ETH. The work at the Philipps University of Marburg was supported by the *Deutsche Forschungsgemeinschaft* (Grants KL1204/1-3 and KL1204/9-1) and the *Graduiertenkolleg* '*Protein*

Function at the Atomic Level'. We also thank Dr. *A. Heine* for his help in protein X-ray analysis, and *P. Hoffmann* and *T. Jansen* for their help in $tRNA^{Tyr}$ production (all Philipps University of Marburg).

Experimental Part

General. Solvents and reagents were reagent-grade, purchased from commercial suppliers, and used without further purification unless otherwise stated. Chloroformamidinium chloride was prepared according to the procedure described in [41]. THF was freshly distilled from sodium benzophenone ketyl. Evaporation *in vacuo* was conducted at H_2O aspirator pressure. All products were dried under high vacuum (h.v., 10^{-2} Torr) before anal. characterization. Column chromatography (CC): SiO_2 *60* (40–63 mm) from *Fluka*, 0–0.3 bar pressure. TLC: SiO_2 *60* F_{245}, *Merck*, visualization by UV light at 254/356 nm. M.p.: *Büchi B540* melting-point apparatus; uncorrected. IR Spectra [cm^{-1}]: *Perkin-Elmer 1600-FT* spectrometer. NMR Spectra (^1H,^{13}C): *Varian Gemini-200*, *Varian Gemini-300*, or *Bruker AMX-500*; spectra were recorded at 298 K with solvent peaks as reference. MS (*m/z* (%)): EI-MS: *VG-TRIBRID* spectrometer at 70 eV; ESI-MS: *Perkin-Elmer Sciex API III* spectrometer; HR-MALDI-MS: *IonSpec Ultima* (2,5-dihydroxybenzoic acid (DHB) matrix). Elemental analyses were performed by the *Mikrolabor* at the *Laboratorium für Organische Chemie*, *ETH-Zürich*. The nomenclature was generated with the computer program *ACD-Name* (*ACD/Labs*) [42].

Crystallization and Soaking. TGT was crystallized and soaked with inhibitors at pH 5.5 as described in [38].

Determination of Kinetic Parameters and Inhibition Constants. The method has been modified according to the initial procedure described by *Reuter et al.* [43] and *Graedler et al.* [13].

Assay Conditions and Workflow. The determination of TGT activity was carried out in 75-µl mixtures containing 150 nM *Z. mobilis* TGT and variable concentrations of *E. coli* $tRNA^{Tyr}$, guanine (7.5% radioactively labeled [8-^{3}H]guanine (*Hartmann Analytik*)), and inhibitor. The assay was performed in 200 mM *HEPES* buffer, pH 7.3, 20 µM $MgCl_2$, and 2.95 µM = 5% *CMC Tween 20* (*Roth*). As some inhibitors were added to the assay soln. dissolved in Me_2SO, due to limited solubility in aq. solns., the final assay soln. contained up to 5% Me_2SO. Reactions were started by adding tRNA and guanine/[8-^{3}H]guanine to the protein soln. Prior to substrate addition, protein and protein/inhibitor mixtures were pre-incubated at 37° for 10 min to allow TGT to adjust to the assay temp. to reach maximum velocity. The mixture was kept at 37°, and 15-µl aliquots were taken at intervals of 1 to 4 min. Aliquots were immediately transferred to glass fiber (*GC-F*) filters (*Whatman*) and quenched with 10% (*w*/*v*) Cl_3CCOOH at 0° for 15 min. Unbound guanine was washed from the filters in 7-min intervals twice with 5% (*w*/*v*) Cl_3CCOOH and twice with EtOH. Filters were dried at 60° for 45 min. ^3H incorporated into tRNA was quantified using liquid scintillation counting. Results from the aliquots were used to calculate initial velocity using *GraFit* [44].

Kinetic Paramters. Michaelis–Menten parameters for tRNA and guanine were determined separately in triplicate. Average values are given in the *Table*. Kinetic parameters for guanine were measured using 75 nM TGT, 15 µM tRNA, and variable concentrations of guanine/[8-^{3}H]guanine (0.5–20 µM). Kinetic parameters for tRNA were measured using 75 nM TGT, 20 µM guanine/[8-^{3}H]guanine, and variable concentrations of tRNA (0.25–15 µM). Initial velocities in *counts per minute* were transferred to [µM/min] using a calibration constant derived from liquid scintillation counting of guanine/[8-^{3}H]guanine solns. with variable concentrations. Kinetic parameters were determined *via* double-reciprocal linearization and linear regression using *GraFit*.

Inhibition Constants for Pure Competitive Inhibition. The inhibition assay was performed using 150 nM TGT, 20 µM guanine/[8-^{3}H]guanine, and tRNA at two concentrations (1 and 1.5 µM). Six reaction mixtures for each tRNA concentration were prepared. To five of them, inhibitor dissolved in Me_2SO (5% final volume) at variable concentrations was added. Initial velocities for the reaction mixtures were determined, and K_{ic} determination was performed using *Dixon* plots. As V_{max} determination is only possible with limited accuracy for independent measurements, a modified equation published by *Graedler et al.* was used to calculate K_{ic} [13]:

$$\frac{v_0}{v_i} \cdot \frac{K_m + [S]}{K_m} = \frac{1}{K_{ic}} \cdot [I] + \left(\frac{[S]}{K_m} + 1\right) \quad (3)$$

Linear regression of data points derived from *Eqn. 3* with *GraFit* results in a straight line with the slope $1/K_{ic}$.

Inhibition Constants for Mixed Inhibition. The inhibition assay was performed using 75 nM TGT, 20 μM guanine/[8-^{3}H]guanine, and variable tRNA concentrations (0.25–15 μM). Kinetic parameters were determined once in the absence of inhibitor (K_m, V_{max}) and twice in the presence of specific inhibitor concentrations [I] to calculate (K_m^{app}, V_{max}^{app}) *via* double-reciprocal linearization and linear regression using *GraFit*. Contributions of K_{ic} and K_{iu} towards pure non-competitive inhibition can be calculated from the following *Eqns. 4* and *5*:

$$K_{iu} = \frac{[I]}{\left(\frac{V_{max}}{V_{max}^{app}}\right) - 1} \quad (4)$$

$$K_{ic} = \frac{[I]}{\left(\frac{K_m^{app} \cdot V_{max}}{K_m \cdot V_{max}^{app}}\right) - 1} \quad (5)$$

The following nomenclature was applied: V_{max}: maximum velocity of uninhibited reaction, v_0: initial velocity at given [S] concentration in the absence of inhibitor, v_i: initial velocity at given [S] concentration in the presence of inhibitor, [S]: tRNA concentration, [I]: inhibitor concentration, K_m: *Michaelis–Menten* constant. Due to the elaborate K_i determination procedure, the average error for the single values is estimated to be in the range of ±25%.

SDS-PAGE Trapping Experiment. 5 μM *Z. mobilis* TGT, 100 μM *E. coli* tRNA^{Tyr}, and 1 mM of the respective inhibitor (dissolved in Me_2SO) in 10 μl of 100 mM *HEPES* buffer, pH 7.3, 20 mM $MgCl_2$, and 5 mM dithiothreitol (DTT) were incubated for 1 h at 25°. A total of 10 μl of SDS loading buffer was added and incubated for another 1 h at 25°. A total of 10 μl of each sample was loaded onto a 15% SDS gel.

Cyclization with Chloroformamidinium Chloride: General Procedure 1 (*GP 1*). A mixture of the anthranilate (1.0 equiv.), chloroformamidinium chloride (1.5 equiv.), and dimethyl sulfone (50.0 equiv.) was heated to 150° for 1.5–3 h. After addition of 25% aq. NH_3 soln. (1–2 ml), the mixture was diluted with H_2O and filtered. The residue was washed with H_2O, MeOH, acetone, and $CHCl_3$. The crude was precipitated from hot DMF and H_2O and dried under h.v. at 80°.

Sonogashira *Cross Coupling: General Procedure 2* (*GP 2*). To a suspension of the iodinated 1*H*-benzimidazole (1.0 equiv.), [$PdCl_2(PPh_3)_2$] (0.1 equiv.), and CuI (0.1 equiv.) in degassed (i-Pr)$_2$NH (0.15M), degassed acetylene (1.5 equiv.) was added. The mixture was heated to 50° for 3 h, and the solvent was removed *in vacuo*. The residue was taken up in sat. aq. NaCl soln. and extracted with CH_2Cl_2 (3×). The combined org. phases were dried ($MgSO_4$) and concentrated *in vacuo*.

Debenzylation and Hydrogenation: General Procedure 3 (*GP 3*). To a soln. of benzylated 1*H*-benzimidazole (1 equiv.) in EtOH (10 mM), Pd/C (0.65–1.0 equiv.) was added, and the mixture was stirred under H_2 (4 bar) for 12 h. The mixture was filtered through *Celite*, concentrated *in vacuo*, and the crude was purified by CC.

*Methyl 1*H*-Benzimidazole-6-carboxylate* (**4**). To a suspension of 1*H*-benzimidazole-6-carboxylic acid (2.0 g, 12.3 mmol) in MeOH (20 ml), $SOCl_2$ (1.4 ml, 19.0 mmol) was added cautiously at 0°, and the mixture was heated to 50° for 12 h. After slow addition of H_2O (35 ml) and removal of MeOH *in vacuo*, the residue was adjusted to pH 6 with sat. aq. $NaHCO_3$ soln. and extracted with AcOEt (3×). The combined org. phases were dried ($MgSO_4$) and concentrated *in vacuo* to give **4** (2.1 g, 96%). Yellow solid. M.p. 133–135°. IR (KBr): 3447*m*, 3110*m*, 2803*m*, 1713*s*, 1623*m*, 1428*m*, 1400*m*, 1312*s*, 1226*m*, 1200*m*, 1081*m*, 886*s*, 824*s*, 785*s*, 768*m*, 745*m*. ^{1}H-NMR (300 MHz, $(CD_3)_2SO$): 12.80 (br. *s*, 1 H); 8.41 (*s*, 1 H); 8.23 (*s*, 1 H); 7.83 (*d*, *J* = 8.4, 1 H); 7.68 (*d*, *J* = 8.4, 1 H); 3.87 (*s*, 3 H). ^{13}C-NMR (75 MHz, $(CD_3)_2SO$): 165.9; 143.4; 136.9; 133.9; 125.2; 124.8; 116.6; 114.8; 52.4. HR-MALDI-MS (DHB): 198.0480 ([*M*+Na]$^+$, $C_9H_8N_2O_2Na^+$, calc. 199.0483). Anal. calc. for $C_9H_8N_2O_2 + 1\ H_2O$ (194.19): C 58.37, H 4.90, N 15.13; found: C 58.25, H 5.15, N 15.25.

*Methyl 5-Nitro-1*H*-benzimidazole-6-carboxylate* (**5**). To fuming HNO_3 (10 ml), conc. H_2SO_4 (10 ml) and subsequently **4** (6.9 g, 39.1 mmol) were added at 0° under stirring. The mixture was heated to 50° for 12 h, cooled to 20°, poured on ice, and filtered. The residue was washed with H_2O, taken up in H_2O/AcOEt, and the pH adjusted to 7–8 with conc. aq. NaOH soln. The aq. phase was extracted with AcOEt (3×), and the combined org. phases were dried ($MgSO_4$) and evaporated *in vacuo* to provide **5** (5.9 g, 68%). Yellow solid. M.p. 100–101° (THF/hexane). IR (KBr): 3106*m*, 2950*m*, 2635*m*, 1733*s*, 1628*m*, 1524*s*, 1468*s*, 1435*s*, 1342*s*, 1311*m*, 1253*s*, 1193*m*, 1107*m*, 896*m*, 860*s*, 813*s*, 793*s*, 781*m*, 761*m*. ^{1}H-NMR (300 MHz, $(CD_3)_2SO$): 8.66 (*s*, 1 H); 8.36 (*s*, 1 H); 8.03 (*s*, 1 H); 3.86 (*s*, 3 H). ^{13}C-NMR (75 MHz, $(CD_3)_2SO$): 165.7; 147.7; 143.2; 139.2; 120.9; 116.4; 113.1; 52.9; 1 C missing. HR-MALDI-MS (DHB): 222.0505 ($[M+H]^+$, $C_9H_8N_3O_4^+$, calc. 222.0515). Anal. calc. for $C_9H_7N_3O_4$ (221.17): C 48.88, H 3.19, N 19.00; found: C 48.93, H 3.33, N 18.87.

*Methyl 1-Benzyl-5-nitro-1*H*-benzimidazole-6-carboxylate* (**6a**) *and Methyl 1-Benzyl-6-nitro-1*H*-benzimidazole-5-carboxylate* (**6b**). To a soln. of **5** (100 mg, 0.45 mmol) in abs. THF (4 ml), NaH (60% in oil, 27 mg, 0.68 mmol) was added at 0°. After stirring for 30 min, BnCl (171 mg, 1.36 mmol) and a cat. amount of Bu_4NI were added, and the mixture was heated to reflux for 12 h. After removal of the solvent *in vacuo*, the residue was taken up in H_2O and extracted with CH_2Cl_2 (3×). The combined org. phases were dried ($MgSO_4$) and concentrated *in vacuo* to give the crude product as brown solid (130 mg, 93%). The regioisomers (**6a**/**6b** 45 : 55) were separated by CC (AcOEt/hexane 4 : 3). Yellowish solids.

Data of **6a**. M.p. 144–146°. IR ($CHCl_3$): 2955*w*, 2253*m*, 1794*w*, 1731*s*, 1628*w*, 1584*w*, 1534*s*, 1462*m*, 1347*s*, 1214*m*, 1120*m*, 651*s*. ^{1}H-NMR (300 MHz, $CDCl_3$): 8.42 (*s*, 1 H); 8.34 (*s*, 1 H); 7.68 (*s*, 1 H); 7.38–7.41 (*m*, 3 H); 7.18–7.22 (*m*, 2 H); 5.45 (*s*, 2 H); 3.90 (*s*, 3 H). ^{13}C-NMR (125 MHz, $CDCl_3$): 166.7; 148.1; 144.6; 136.0; 135.2; 134.2; 129.6; 129.2; 128.9; 127.4; 117.7; 112.1; 53.5; 49.7. HR-MALDI-MS (DHB): 312.0973 ($[M+H]^+$, $C_{16}H_{14}N_3O_4^+$, calc. 312.0984).

Data of **6b**. M.p. 135–137°. IR ($CHCl_3$): 3020*w*, 1730*s*, 1628*w*, 1533*s*, 1456*m*, 1347*s*, 1120*m*, 897*w*. ^{1}H-NMR (500 MHz, $CDCl_3$): 8.32 (br. *s*, 1 H); 8.19 (*s*, 1 H); 8.02 (*s*, 1 H); 7.36–7.41 (*m*, 3 H); 7.18–7.20 (*m*, 2 H); 5.44 (*s*, 2 H); 3.93 (*s*, 3 H). ^{13}C-NMR (125 MHz, $CDCl_3$): 166.0; 148.4; 144.5; 135.1; 134.1; 129.6; 129.2; 128.7; 127.4; 123.4; 122.4; 107.9; 53.5; 49.6.

*Methyl 5-Amino-1-benzyl-1*H*-benzimidazole-6-carboxylate* (**7a**) *and Methyl 6-Amino-1-benzyl-1*H*-benzimidazole-5-carboxylate* (**7b**). To a soln. of **6a** (50 mg, 0.16 mmol) in AcOH (10 ml) and H_2O (3 ml), Zn (105 mg, 1.6 mmol) was added portionwise at 20°. After stirring for 3 h at 20°, the mixture was filtered through *Celite*, and the filtrate was concentrated *in vacuo*. The residue was taken up in H_2O and adjusted to pH 7–8 with conc. aq. NaOH soln. The precipitated Zn salts were removed by filtration through *Celite*, and the aq. phase was extracted with CH_2Cl_2 (3×). The org. phases were dried ($MgSO_4$) and evaporated *in vacuo*. CC (CH_2Cl_2/MeOH 96 : 4) provided **7a** (38 mg, 85%). Yellow solids.

Data of **7a**. M.p. 172–174° ($CHCl_3$/hexane). IR ($CHCl_3$): 3382*w*, 2956*m*, 1692*s*, 1640*m*, 1591*s*, 1293*m*, 1102*m*. ^{1}H-NMR (300 MHz, $CDCl_3$): 8.05 (*s*, 1 H); 7.89 (*s*, 1 H); 7.35–7.37 (*m*, 3 H); 7.19–7.22 (*m*, 2 H); 7.06 (*s*, 1 H); 5.31 (*s*, 2 H); 3.87 (*s*, 3 H). ^{13}C-NMR (75 MHz, $CDCl_3$): 168.7; 149.1; 147.0; 146.9; 135.5; 129.3; 128.8; 128.5; 127.3; 112.9; 109.4; 105.3; 51.9; 48.9. HR-MALDI-MS (DHB): 282.1270 ($[M+H]^+$, $C_{16}H_{16}N_3O_2^+$, calc. 282.1243). Anal. calc. for $C_{16}H_{15}N_3O_2$ (281.31): C 68.31, H 5.37, N 14.94; found: C 68.18, H 5.52, N 15.09.

Through reduction of the regioisomeric mixture of **6a**/**6b**, the other regioisomer **7b** was obtained.

Data of **7b**. M.p. 158–160°. IR ($CHCl_3$): 3500*w*, 3378*w*, 2253*m*, 1688*m*, 1637*m*, 1591*m*, 1301*m*, 1208*s*, 905*s*, 665*s*. ^{1}H-NMR (300 MHz, $CDCl_3$): 8.38 (*s*, 1 H); 7.94 (*s*, 1 H); 7.26–7.32 (*m*, 3 H); 7.14–7.17 (*m*, 2 H); 6.43 (*s*, 1 H); 5.23 (*s*, 2 H); 4.63 (br. *s*, 2 H); 3.89 (*s*, 3 H). ^{13}C-NMR (75 MHz, $CDCl_3$): 168.7; 147.3; 143.8; 139.0; 136.1; 135.1; 129.0; 128.2; 126.9; 123.8; 108.7; 94.7; 51.8; 48.6.

*Methyl 5-Amino-1-benzyl-4-iodo-1*H*-benzimidazole-6-carboxylate* (**8**). To a degassed soln. of **7a** (2.7 g, 9.6 mmol) in CH_2Cl_2 (150 ml), an aq. $NaHCO_3$ soln. (0.22M, 75 ml) and I_2 (2.9 g, 11.5 mmol) were added, and the mixture was stirred for 3 h at 20°. After addition of sat. aq. Na_2SO_3 soln. (20 ml), the org. layer was separated, and the aq. phase was extracted with CH_2Cl_2 (3×). The combined org. phases were dried ($MgSO_4$) and evaporated *in vacuo* to give a dark red powder (3.7 g, 95%). For anal. purposes, a small amount of **8** was purified by CC (AcOEt/hexane 1 : 1). Yellow solid. M.p. 167–169° (THF/hexane). IR ($CHCl_3$): 3476*w*, 3360*w*, 2954*w*, 1692*s*, 1628*m*, 1585*s*, 1492*m*, 1293*m*, 1120*m*. ^{1}H-NMR (300 MHz, $CDCl_3$): 8.08 (*s*, 1 H); 7.89 (*s*, 1 H); 7.34–7.38 (*m*, 3 H); 7.17–7.20 (*m*, 2 H); 5.32 (*s*, 2 H); 3.88

(*s*, 3 H). ^{13}C-NMR (75 MHz, $CDCl_3$): 167.6; 150.2; 146.1; 146.0; 134.8; 129.0; 128.3; 126.9; 125.0; 113.4; 108.9; 75.6; 52.1; 49.2. HR-MALDI-MS (DHB): 408.0196 ($[M+H]^+$, $C_{16}H_{15}IN_3O_2^+$, calc. 408.0209). Anal. calc. for $C_{16}H_{14}IN_3O_2$ (407.21): C 47.19, H 3.47, N 10.32; found: C 47.34, H 3.59, N 10.13.

*Methyl 5-Amino-1*H*-benzimidazole-6-carboxylate* (**9**). To a soln. of **5** (13.0 g, 59 mmol) in AcOH (500 ml), Pd/C (10%, 1.2 g) was added, and the mixture was heated to reflux for 1 h under H_2 and subsequently for 12 h at 20°. After filtration through *Celite*, the solvent was evaporated *in vacuo*. CC (CH_2Cl_2/MeOH 96:4) provided **9** (11.01 g, 98%). White solid. M.p. 169–170° ($CHCl_3$/hexane). IR (KBr): 3490*m*, 3379*m*, 2951*w*, 2763*w*, 1696*s*, 1647*m*, 1585*s*, 1435*m*, 1304*s*, 1242*m*, 1195*m*, 1141*w*, 888*w*, 853*w*, 815*w*, 793*s*. ^{1}H-NMR (300 MHz, $(CD_3)_2SO$): 8.13 (*s*, 1 H); 8.02 (*s*, 1 H); 6.84 (*s*, 1 H); 3.85 (*s*, 3 H). ^{13}C-NMR (75 MHz, $(CD_3)_2SO$): 169.5; 148.6; 143.6; 141.3; 133.1; 120.4; 109.5; 98.8; 51.7. ESI-MS: 191.1 (100, M^+), 159.0 (96), 131.0 (65), 105.0 (21). Anal. calc. for $C_9H_9N_3O_2$ (191.19): C 56.54, H 4.74, N 21.98; found: C 56.27, H 4.79, N 21.78.

*6-Amino-1,7-dihydro-8*H*-imidazo[4,5-*g*]quinazolin-8-one* (lin-*Benzoguanine*; **2**). *GP 1* with **9** (250 mg, 1.31 mmol), chloroformamidinium chloride (225 mg, 1.96 mmol), and dimethylsulfone (2.5 g) provided **2** (84 mg, 32%). White solid. M.p. >300° (DMF/H_2O). Spectroscopic data were in agreement with those reported in [45].

*Methyl 5-Amino-1-benzyl-4-(2-phenylethynyl)-1*H*-benzimidazole-6-carboxylate* (**10a**). *GP 2* with **8** (100 mg, 0.24 mmol), $[PdCl_2(PPh_3)_2]$ (17 mg, 0.02 mmol), CuI (4.7 mg, 0.02 mmol), and ethynylbenzene (41 µl, 0.37 mmol). CC (CH_2Cl_2/MeOH 99:1) provided **10a** (74 mg, 81%). Yellow powder. M.p. 188–190°. IR ($CHCl_3$): 3491*w*, 3370*w*, 2954*w*, 1692*s*, 1592*m*, 1269*m*, 1124*m*. ^{1}H-NMR (300 MHz, $CDCl_3$): 8.06 (*s*, 1 H); 7.88 (*s*, 1 H); 7.63–7.66 (*m*, 2 H); 7.32–7.37 (*m*, 6 H); 7.16–7.19 (*m*, 2 H); 5.33 (*s*, 2 H); 3.88 (*s*, 3 H). ^{13}C-NMR (75 MHz, $CDCl_3$): 168.0; 148.4; 146.3; 134.8; 131.7; 129.0; 128.4; 128.2; 128.1 (2×); 126.9; 125.5; 123.1; 113.6; 108.3; 100.5; 98.0; 81.9; 51.9; 49.0. HR-MALDI-MS (DHB): 382.1547 ($[M+H]^+$, $C_{24}H_{20}N_3O_2^+$, calc. 382.1556).

*Methyl 5-Amino-1-benzyl-4-[2-(4-methylphenyl)ethynyl]-1*H*-benzimidazole-6-carboxylate* (**10b**). *GP 2* with **8** (500 mg, 1.23 mmol), $[PdCl_2(PPh_3)_2]$ (86 mg, 0.12 mmol), CuI (23 mg, 0.12 mmol), and 1-ethynyl-4-methylbenzene (234 µl, 1.84 mmol). CC (CH_2Cl_2/MeOH 99.25:0.75) provided **10b** (456 mg, 94%). Dark-yellow powder. M.p. 212–214° ($CHCl_3$/hexane). IR ($CHCl_3$): 3479*m*, 3375*m*, 2805*m*, 1688*s*, 1636*s*, 1588*s*, 1420*s*, 1310*s*, 1277*m*, 1209*s*, 1102*m*, 1068*m*, 949*w*, 788*m*, 627*m*. ^{1}H-NMR (300 MHz, $CDCl_3$): 8.00 (*s*, 1 H); 7.86 (*s*, 1 H); 7.53 (*d*, *J* = 8.1, 2 H); 7.33–7.38 (*m*, 3 H); 7.14–7.18 (*m*, 4 H); 6.38 (br. *s*, 2 H); 5.32 (*s*, 2 H); 3.88 (*s*, 3 H); 2.37 (*s*, 3 H). ^{13}C-NMR (75 MHz, $CDCl_3$): 168.1; 148.4; 148.3; 146.8; 138.3; 135.1; 131.5; 129.0; 128.9; 128.3; 126.9; 125.7; 120.1; 113.3; 108.1; 100.7; 98.5; 81.5; 51.9; 48.9; 21.7. HR-MALDI-MS (DHB): 396.1712 ($[M+H]^+$, $C_{25}H_{22}N_3O_2^+$, calc. 396.1712). Anal. calc. for $C_{25}H_{21}N_3O_2$ (395.45): C 75.93, H 5.35, N 10.63; found: C 75.97, H 5.54, N 10.55.

*Methyl 5-Amino-1-benzyl-4-[2-(4-methoxyphenyl)ethynyl]-1*H*-benzimidazole-6-carboxylate* (**10c**). *GP 2* with **8** (500 mg, 1.23 mmol), $[PdCl_2(PPh_3)_2]$ (86 mg, 0.12 mmol), CuI (23 mg, 0.12 mmol), and 1-ethynyl-4-methoxylbenzene (234 µl, 1.84 mmol). CC (CH_2Cl_2/MeOH 95.5:0.5) provided **10c** (380 mg, 75%). Dark-yellow powder. M.p. 186–188°. IR ($CHCl_3$): 3484*w*, 3372*w*, 3008*m*, 2358*m*, 1692*s*, 1607*s*, 1564*m*, 1492*s*, 1438*m*, 1290*s*, 1125*m*, 968*w*, 833*m*. ^{1}H-NMR (300 MHz, $CDCl_3$): 8.00 (*s*, 1 H); 7.72 (*s*, 1 H); 7.46 (*d*, *J* = 8.6, 2 H); 7.25–7.28 (*m*, 3 H); 7.08–7.11 (*m*, 2 H); 6.77 (*d*, *J* = 8.6, 2 H); 6.33 (br. *s*, 2 H); 5.21 (*s*, 2 H); 3.80 (*s*, 3 H); 3.74 (*s*, 3 H). ^{13}C-NMR (75 MHz, $CDCl_3$): 168.0; 159.4; 148.1; 146.8; 146.1; 135.0; 133.0; 128.9; 128.2; 126.8; 125.6; 115.2; 113.7; 113.2; 108.0; 100.5; 98.4; 80.9; 55.3; 51.8; 48.8. HR-MALDI-MS (DHB): 412.1661 ($[M+H]^+$, $C_{25}H_{22}N_3O_3^+$, calc. 412.1661).

*Methyl 5-Amino-4-(2-phenylethyl)-1*H*-benzimidazole-6-carboxylate* (**11a**). *GP 3* with **10a** (600 mg, 1.57 mmol) and Pd/C (600 mg). CC (CH_2Cl_2/MeOH 97:3) provided **11a** (280 mg, 60%). White powder. M.p. 200–202°. IR (KBr): 3506*w*, 3392*m*, 3138*s*, 2951*s*, 2588*m*, 1730*m*, 1700*s*, 1583*s*, 1425*s*, 1307*s*, 1204*s*, 1001*m*, 602*m*. ^{1}H-NMR (300 MHz, CD_3OD): 8.12 (*s*, 1 H); 8.00 (*s*, 1 H); 7.12–7.23 (*m*, 5 H); 3.89 (*s*, 3 H); 3.12 (*t*, *J* = 7.8, 2 H); 2.90 (*t*, *J* = 7.8, 2 H). ^{13}C-NMR (125 MHz, $(CD_3)_2SO$ + 2 drops of CF_3CO_2D): 168.1; 147.5; 140.7; 134.9; 128.6; 128.1; 126.1; 121.3; 115.2; 117.8; 113.6; 109.7; 51.5; 32.6; 27.4. HR-MALDI-MS (DHB): 296.1397 ($[M+H]^+$, $C_{17}H_{18}N_3O_2^+$, calc. 296.1399).

*Methyl 5-Amino-4-[2-(4-methylphenyl)ethyl]-1*H*-benzimidazole-6-carboxylate* (**11b**). *GP 3* with **10b** (300 mg, 0.76 mmol) and Pd/C (200 mg). CC (CH_2Cl_2/MeOH 97:3) provided **11b** (131 mg, 56%). White powder. M.p. 238–240°. IR (KBr): 3473*w*, 3364*w*, 2949*w*, 1688*s*, 1620*s*, 1555*s*, 1496*s*, 1425*m*, 1342*s*, 1267*s*,

1229*s*, 1065*s*, 812*s*. ^{1}H-NMR (300 MHz, CD_3OD): 8.11 (*s*, 1 H); 8.00 (br. *s*, 1 H); 7.10 (*d*, *J* = 7.8, 2 H); 7.02 (*d*, *J* = 7.8, 2 H); 3.88 (*s*, 3 H); 3.08 (*t*, *J* = 6.6, 2 H); 2.27 (*t*, *J* = 6.6, 2 H); 2.26 (*s*, 3 H). ^{13}C-NMR (125 MHz, $(CD_3)_2SO$): 168.4; 147.3; 142.7; 138.5; 135.5; 135.3; 129.3; 129.2; 122.0; 115.7; 110.9; 110.7; 52.9; 32.9; 27.6; 21.3. HR-MALDI-MS (DHB): 310.1547 ($[M+H]^+$, $C_{18}H_{20}N_3O_2^+$, calc. 310.1556).

*Methyl 5-Amino-4-[2-(4-methoxyphenyl)ethyl]-1*H*-benzimidazole-6-carboxylate* (**11c**). *GP 3* with **10c** (350 mg, 0.85 mmol) and Pd/C (10%, 550 mg), reaction time: 7 d. CC (CH_2Cl_2/MeOH 97:3) provided **11c** (122 mg, 44%). White powder. M.p. 208–209°. IR ($CHCl_3$): 3463*w*, 3374*w*, 3002*w*, 2953*w*, 1685*s*, 1635*m*, 1610*w*, 1581*w*, 1512*s*, 1437*m*, 1313*m*, 1304*m*, 1248*s*, 1220*s*, 1200*s*. ^{1}H-NMR (300 MHz, CD_3OD): 8.10 (*s*, 1 H); 7.99 (*s*, 1 H); 7.12 (*d*, *J* = 8.4, 2 H); 6.76 (*d*, *J* = 8.4, 2 H); 3.88 (*s*, 3 H); 3.73 (*s*, 3 H); 3.08 (*t*, *J* = 7.8, 2 H); 2.84 (*t*, *J* = 7.8, 2 H). ^{13}C-NMR (75 MHz, CD_3OD): 169.4; 158.3; 144.6; 142.8; 133.7; 129.4; 129.2; 118.1; 116.8; 113.5; 110.0; 109.1; 54.4; 50.9; 32.8; 28.3. HR-MALDI-MS (DHB): 326.1499 ($[M+H]^+$, $C_{18}H_{20}N_3O_3^+$, calc.326.1505).

*6-Amino-4-(2-phenylethyl)-1,7-dihydro-8*H*-imidazo[4,5-*g*]quinazolin-8-one* (**12a**). *GP 1* with **11a** (130 mg, 0.44 mmol) and chloroformamidinium chloride (76 mg, 0.66 mmol). Greenish solid (47 mg, 35%). M.p. >300° (dec.). IR (KBr): 3468*w*, 3374*m*, 3109*s*, 2927*m*, 1649*s*, 1600*s*, 1494*s*, 1280*s*, 1121*m*, 889*m*, 702*m*. ^{1}H-NMR (300 MHz, $(CD_3)_2SO$): 12.46 (br. *s*, 1 H); 10.86 (br. *s*, 1 H); 8.30 (*s*, 1 H); 8.03 (*s*, 1 H); 7.18–7.38 (*m*, 5 H); 6.15 (br. *s*, 2 H); 3.35 (*t*, *J* = 9.0, 2 H); 2.89 (*t*, *J* = 9.0, 2 H). ^{13}C-NMR (125 MHz, $(CD_3)_2SO$ + 2 drops of CF_3CO_2D): 160.1; 151.3; 145.2; 140.2; 137.7; 133.5; 130.0; 128.7; 128.0; 126.2; 115.8; 113.9; 111.8; 34.4; 26.5. HR-MALDI-MS (DHB): 306.1346 ($[M+H]^+$, $C_{17}H_{16}N_5O^+$, calc. 306.1355).

*6-Amino-4-[2-(4-methylphenyl)ethyl]-1,7-dihydro-8*H*-imidazo[4,5-*g*]quinazolin-8-one* (**12b**). *GP 1* with **11b** (80 mg, 0.26 mmol) and chloroformamidinium chloride (45 mg, 0.39 mmol). Yellow solid (50 mg, 60%). M.p. >300° (dec.). IR (KBr): 3467*w*, 3380*m*, 3108*m*, 2921*m*, 1649*s*, 1610*s*, 1513*s*, 1415*s*, 1369*s*, 1281*m*, 1123*w*, 808*w*, 795*w*. ^{1}H-NMR (300 MHz, $(CD_3)_2SO$): 12.53 (br. *s*, 1 H); 10.78 (br. *s*, 1 H); 8.26 (*s*, 1 H); 8.05 (*s*, 1 H); 7.25 (*d*, *J* = 7.8, 2 H); 7.09 (*d*, *J* = 7.8, 2 H); 6.09 (br. *s*, 2 H); 3.26 (*t*, *J* = 8.1, 2 H); 2.81 (*t*, *J* = 8.1, 2 H); 2.25 (*s*, 3 H). ^{13}C-NMR (125 MHz, $(CD_3)_2SO$): 160.2; 151.4; 145.2; 138.0; 137.2; 135.1; 133.4; 130.3; 128.6; 128.5; 116.0; 113.8; 111.8; 34.1; 26.6; 20.6. HR-MALDI-MS (DHB): 320.1504 ($[M+H]^+$, $C_{18}H_{18}N_5O^+$, calc. 320.1511).

*6-Amino-4-[2-(methoxyphenyl)ethyl]-1,7-dihydro-8*H*-imidazo[4,5-*g*]quinazolin-8-one* (**12c**). *GP 1* with **11c** (92 mg, 0.28 mmol) and chloroformamidinium chloride (49 mg, 0.42 mmol). Yellow solid (62 mg, 66%). M.p. >300°. IR (KBr): 3382*m*, 3111(sh), 2918*m*, 1651*s*, 1615*s*, 1575*s*, 1511*s*, 1413*m*, 1393*m*, 1372*m*, 1243*s*. ^{1}H-NMR (300 MHz, $(CD_3)_2SO$): 12.41 (br. *s*, 1 H); 10.84 (br. *s*, 1 H); 8.30 (*s*, 1 H); 8.02 (*s*, 1 H); 7.27 (*d*, *J* = 8.4, 2 H); 6.85 (*d*, *J* = 8.4, 2 H); 6.15 (br. *s*, 2 H); 3.72 (*s*, 3 H); 3.33 (*t*, *J* = 8.0, 2 H); 2.82 (*t*, *J* = 8.0, 2 H). ^{13}C-NMR (75 MHz, $(CD_3)_2SO$): 160.0; 157.4; 151.0; 145.1; 138.3; 133.2; 132.1; 130.6; 129.4; 113.3; 113.2; 111.6; 109.6; 54.9; 33.7; 26.8. HR-MALDI-MS (DHB): 336.1461 ($[M+H]^+$, $C_{18}H_{18}N_5O_2^+$, calc. 336.1461).

*4-(2-Phenylethyl)-1,7-dihydro-8*H*-imidazo[4,5-*g*]quinazolin-8-one* (**13**). A mixture of **11a** (100 mg, 0.34 mmol) and formamidinium acetate (46 mg, 0.44 mmol) in EtOH (6 ml) was heated to reflux for 2 d. Another portion of formamidinium acetate was added (46 mg, 0.44 mmol), and the mixture was heated for further 2 d. After removal of the solvent *in vacuo*, the residue was washed with H_2O and CH_2Cl_2. CC (CH_2Cl_2/MeOH 95:5) provided **13** (80 mg, 81%). White solid. M.p. >300°. IR (KBr): 3425 (sh), 3159*m*, 3061*m*, 3025*m*, 2918*m*, 1661*s*, 1615*s*, 1583*m*, 1492*m*, 1454*m*, 1411*s*, 1281*m*, 1185*m*. ^{1}H-NMR (300 MHz, CD_3OD): 8.39 (*s*, 2 H); 8.02 (*s*, 1 H); 7.08–7.24 (*m*, 5 H); 3.65 (*t*, *J* = 8.0, 2 H); 3.00 (*t*, *J* = 8.0, 2 H). ^{13}C-NMR (125 MHz, $(CD_3)_2SO$ + 2 drops of CF_3CO_2D): 161.0; 144.9; 144.0; 142.8; 141.1; 135.1; 130.1; 128.3; 128.1; 125.9; 124.7; 120.7; 109.6; 35.4; 27.7. HR-MALDI-MS (DHB): 291.1238 ($[M+H]^+$, $C_{17}H_{15}N_4O^+$, calc. 291.1246).

*Methyl 5-Amino-1-benzyl-4-phenyl-1*H*-benzimidazole-6-carboxylate* (**14**). A suspension of **8** (500 mg, 1.22 mmol), phenylboronic acid (157 mg, 1.22 mmol), K_2CO_3 (279 mg, 2.02 mmol), and $[Pd(PPh_3)_4]$ (94 mg, 0.08 mmol) in EtOH (10 ml), toluene (5 ml), and H_2O (5 ml) was heated to 80° for 2 d. After cooling to 20°, the mixture was treated with sat. aq. NH_4Cl soln. and extracted with AcOEt (3×). The combined org. phases were dried ($MgSO_4$) and evaporated *in vacuo*. CC (CH_2Cl_2/MeOH 95.25:0.75) provided **14** (377 mg, 87%). Yellow solid. M.p. 70–72°. IR ($CHCl_3$): 3491*w*, 3382*w*, 3027*m*, 3031*m*, 1690*s*, 1627*m*, 1569*m*, 1497*s*, 1437*m*, 1419*m*, 1332*m*, 1123*w*. ^{1}H-NMR (300 MHz,

$(CD_3)_2SO$): 8.32 (*s*, 1 H); 7.93 (*s*, 1 H); 7.24–7.51 (*m*, 10 H); 5.78 (br. *s*, 2 H); 5.46 (*s*, 2 H); 3.79 (*s*, 3 H). ^{13}C-NMR (75 MHz, $CDCl_3$): 169.0; 147.7; 147.0; 143.8; 135.7; 135.0; 130.7; 129.4; 129.3; 128.5; 128.0; 127.2; 126.7; 117.6; 112.3; 109.1; 52.0; 48.9. HR-MALDI-MS (DHB): 358.1553 ($[M+H]^+$, $C_{22}H_{20}N_3O_2^+$, calc. 358.1556).

*Methyl 5-Amino-4-phenyl-1*H*-benzimidazole-6-carboxylate* (**15**). A suspension of **14** (0.35 g, 0.98 mmol) and Pd/C (10%, 0.35 g) in EtOH (18 ml) and AcOH (2 ml) was hydrogenated (1 bar) for 24 h at 20°. The mixture was filtered through *Celite*, and the solvent was removed *in vacuo*. The residue was taken up in CH_2Cl_2/sat. aq. $NaHCO_3$ soln. and extracted with CH_2Cl_2 (3×). The combined org. phases were dried ($MgSO_4$) and concentrated *in vacuo*. CC (CH_2Cl_2/MeOH 98.6:1.4) provided **15** (205 mg, 78%). Yellow solid. M.p. 198–201°. IR ($CHCl_3$): 3452*w*, 3374*w*, 2996*w*, 1688*s*, 1634*m*, 1603*w*, 1576*m*, 1501*w*, 1437*m*, 1417*w*, 1372*w*, 1329*s*. ^{1}H-NMR (300 MHz, $CDCl_3$): 11.80 (br. *s*, 1 H) 8.27 (*s*, 1 H); 7.49 (*s*, 1 H); 7.32–7.41 (*m*, 4 H); 7.22–7.26 (*m*, 1 H); 5.67 (br. *s*, 2 H); 3.85 (*s*, 3 H). ^{13}C-NMR (75 MHz, $CDCl_3$): 169.0; 143.8; 142.1; 138.6; 134.3; 132.7; 129.9; 129.4; 127.9; 120.6; 110.5; 108.5; 51.6. HR-MALDI-MS (DHB): 268.1084 ($[M+H]^+$, $C_{15}H_{14}N_3O_2^+$, calc. 268.1086).

*6-Amino-4-phenyl-1,7-dihydro-8*H*-imidazo[4,5-*g*]quinazolin-8-one* (**16**). *GP 1* with **15** (195 mg, 0.73 mmol) and chloroformamidinium chloride (126 mg, 1.09 mmol) provided **16** (76 mg, 38%). Yellow solid. M.p. >300°. IR (KBr): 3310*m*, 3131*s*, 1651*s*, 1605*s*, 1574*s*, 1498*m*, 1387*m*, 1283*w*. ^{1}H-NMR (300 MHz, $(CD_3)_2SO$ + 2 drops of D_2O + 5 drops of CF_3CO_2D): 9.03 (*s*, 1 H); 8.40 (*s*, 1 H); 7.54–7.69 (*m*, 5 H). ^{13}C-NMR (125 MHz, $(CD_3)_2SO$ + 2 drops CF_3CO_2D): 160.2; 151.4; 146.6; 140.7; 133.6; 131.2; 131.1; 130.6; 129.4; 129.1; 116.4; 113.3; 112.3. HR-MALDI-MS (DHB): 278.1033 ($[M+H]^+$, $C_{15}H_{12}N_5O^+$, calc. 278.1042).

*6-Amino-3-benzyl-3,7-dihydro-8*H*-imidazo[4,5-*g*]quinazolin-8-one* (**17a**). *GP 1* with **7b** (200 mg, 0.71 mmol) and chloroformamidinium chloride (123 mg, 1.07 mmol) provided **17a** (176 mg, 85%). White solid. M.p. >300°. IR (KBr): 3107*m*, 2745*m*, 1699*s*, 1394*s*, 1559*m*, 1497*m*, 1455*m*, 1331*m*, 1211*w*, 704*m*. ^{1}H-NMR (300 MHz, $(CD_3)_2SO$): 10.81 (br. *s*, 1 H); 8.46 (*s*, 1 H); 8.14 (*s*, 1 H); 7.28–7.38 (*m*, 5 H); 7.16 (*s*, 1 H); 6.13 (br. *s*, 2 H); 5.47 (*s*, 2 H). ^{13}C-NMR (125 MHz, $(CD_3)_2SO$ + 2 drops CF_3CO_2D): 162.4; 151.4 (2×); 148.2; 141.1; 139.4; 136.9; 129.5; 128.6; 128.1; 118.2; 112.8; 100.7; 48.6. HR-MALDI-MS (DHB): 292.1195 ($[M+H]^+$, $C_{16}H_{14}N_5O^+$, calc. 292.1198).

*Methyl 6-Nitro-1-(2-phenylethyl)-1*H*-benzimidazole-5-carboxylate* (**18**). To a soln. of **6** (1.0 g, 4.52 mmol) in abs. THF (4 ml), NaH (60% in oil, 217 mg, 5.42 mmol) was added at 0°. After 20 min stirring, 2-phenylethyl chloride (1.83 ml, 13.5 mmol) was added, and the mixture was heated to reflux for 12 h. After removal of the solvent *in vacuo*, the residue was taken up in H_2O and extracted with CH_2Cl_2 (3×). The combined org. phases were dried ($MgSO_4$) and concentrated *in vacuo*. The regioisomers were separated by CC (AcOEt/hexane 7:3). Yellow oil. IR ($CHCl_3$): 3563 (sh), 3361 (sh), 3034*w*, 2993*w*, 2954*m*, 1737*s*, 1731*s*, 1625*m*, 1589*m*, 1535*s*, 1492*m*, 1438*s*, 1380*s*, 1346*s*, 1285*s*. ^{1}H-NMR (300 MHz, $CDCl_3$): 8.07 (*s*, 1 H); 7.82 (*s*, 1 H); 7.81 (*s*, 1 H); 7.22–7.27 (*m*, 3 H); 6.93–6.97 (*m*, 2 H); 4.49 (*t*, *J* = 6.6, 2 H); 3.94 (*s*, 3 H); 3.15 (*t*, *J* = 6.6, 2 H). ^{13}C-NMR (75 MHz, $CDCl_3$): 166.3; 147.9; 145.4; 144.0; 136.6; 133.8; 128.9; 128.4; 127.3; 122.2; 121.9; 107.2; 53.2; 47.4; 36.5. HR-MALDI-MS (DHB): 326.1138 ($[M+H]^+$, $C_{17}H_{16}N_3O_4^+$, calc. 326.1141).

*Methyl 6-Amino-1-(2-phenylethyl)-1*H*-benzimidazole-5-carboxylate* (**19**). A suspension of **18** (292 mg, 0.90 mmol) and Pd/C (10%, 30 mg) in AcOH (10 ml) was hydrogenated (1 bar) for 12 h at 20°. The mixture was filtrated through *Celite*, and the solvent was removed *in vacuo*. The residue was taken up in CH_2Cl_2/sat. aq. $NaHCO_3$ soln. and extracted with CH_2Cl_2 (4×). The combined org. phases were dried ($MgSO_4$) and concentrated *in vacuo*. CC (AcOEt) provided **19** (216 mg, 81%). Yellow solid. M.p. 153–155°. IR ($CHCl_3$): 3498*m*, 3378*m*, 2993*m*, 2952*m*, 1692*s*, 1637*s*, 1591*s*, 1504*m*, 1454*s*, 1437*s*, 1360*m*, 1302*s*, 1244*m*. ^{1}H-NMR (300 MHz, $CDCl_3$): 8.34 (*s*, 1 H); 7.40 (*s*, 1 H); 7.20–7.42 (*m*, 3 H); 6.96–7.00 (*m*, 2 H); 6.47 (*s*, 1 H); 5.60 (br. *s*, 2 H); 4.20 (*t*, *J* = 6.9, 2 H); 3.87 (*s*, 3 H); 3.04 (*t*, *J* = 6.9, 2 H). ^{13}C-NMR (75 MHz, $CDCl_3$): 169.2; 147.5; 144.0; 138.9; 137.7; 136.4; 129.1; 128.9; 127.3; 124.1; 108.8; 94.6; 51.9; 46.7; 36.0. HR-MALDI-MS (DHB): 296.1396 ($[M+H]^+$, $C_{17}H_{18}N_3O_2^+$, calc. 296.1399).

*6-Amino-3-(2-phenylethyl)-3,7-dihydro-8*H*-imidazo[4,5-*g*]quinazolin-8-one* (**17b**). *GP 1* with **19** (0.20 g, 0.68 mmol) and chloroformamidinium chloride (0.12 g, 1.02 mmol) provided **17b** (177 mg, 85%). White solid. M.p. >300°. IR (KBr): 3463*m*, 3096*m*, 2922*w*, 1651*s*, 1557*s*, 1506*s*, 1448*m*, 1358*m*.

^{1}H-NMR (300 MHz, $(CD_3)_2SO$): 10.98 (br. *s*, 1 H); 8.11 (*s*, 1 H); 8.07 (*s*, 1 H); 7.30 (*s*, 1 H); 7.13–7.25 (*m*, 5 H); 6.28 (br. *s*, 2 H); 4.46 (*t*, $J=6.9$, 2 H); 3.09 (*t*, $J=6.9$, 2 H). ^{13}C-NMR (75 MHz, $(CD_3)_2SO$): 162.8; 150.2; 150.1; 146.1; 139.4; 138.9; 137.9; 128.6; 128.2; 126.3; 116.2; 113.0; 102.5; 45.4; 35.0. HR-MALDI-MS (DHB): 306.1353 ($[M+H]^+$, $C_{17}H_{16}N_5O^+$, calc. 306.1355).

X-Ray Crystal Structures. Cell determination and data collection for all compounds were performed on a *Bruker Kappa CCD* instrument, and cell refinement and data reduction with the programs Scalepack and Denzo [46].

Compound **7b**. Crystals were grown in a soln. of THF with an upper layer of hexane. X-Ray crystal data for $C_{16}H_{15}N_3O_2$ (M_r 281.315): trigonal space group *R*3 (hexagonal setting), $D_x=1.299$ g/cm^{-3}, $Z=18$, $a=28.3050(4)$, $b=28.3050(9)$, $c=9.3331(3)$ Å, $V=6475.6$ (3) Å^3, MoK_α radiation, $\lambda=0.71073$ Å, $0.998^\circ\leq\theta\leq29.575^\circ$, 11415 measured reflections, 6403 independent reflections ($R_{int}=0.039$), $T=298$ K. The structure was solved by direct methods (SIR97, [47]) and refined by full-matrix least-squares analysis [48]. All non-H-atoms were refined anisotropically, H-atoms were included in the structure factor calculation, with positions based on stereochemical considerations. Final agreement factors: $R(gt)=0.0513$, $wR(gt)=0.1370$ for 379 parameters and 4776 observed reflections with $I>2\sigma(I)$. *Cambridge Crystallographic Data Centre* deposition No. CCDC-256502.

Compound **8**. Crystals were grown by slow diffusion of hexane into a soln. of **8** in THF. X-Ray crystal data for $C_{16}H_{14}IN_3O_2$ (M_r 407.207): Monoclinic space group $P2_1/c$, $D_x=1.754$ g/cm^{-3}, $Z=4$, $a=10.2926(2)$, $b=6.87470(10)$, $c=22.0059(4)$ Å, $V=1542.27(5)$ Å^3, MoK_α radiation, $\lambda=0.71073$ Å, $0.998^\circ\leq\theta\leq30.508^\circ$, 9089 measured reflections, 4683 independent reflections ($R_{int}=0.028$), $T=298$ K. The structure was solved by direct methods (SIR97, [47]) and refined by full-matrix least-squares analysis (SHELXL-97). All non-H-atoms were refined anisotropically, H-atoms were included in the structure factor calculation, with positions based on stereochemical considerations. Final agreement factors: $R(gt)=0.0445$, $wR(gt)=0.1438$ for 199 parameters and 3008 observed reflections with $I>2\sigma(I)$. *Cambridge Crystallographic Data Centre* deposition No. CCDC-256501.

Compound **10b**. Crystals were grown by slow diffusion of hexane into a soln. of **8** in $CHCl_3$. X-Ray crystal data for $C_{25}H_{21}N_3O_2$ (M_r 395.462): Monoclinic space group $P2_1/n$, $D_x=1.275$ g/cm^{-3}, $Z=4$, $a=12.7484(1)$, $b=6.2552(2)$, $c=26.2696(5)$ Å, $V=2060.49(8)$ Å^3, MoK_α radiation, $\lambda=0.71073$ Å, $0.998^\circ\leq\theta\leq25.350^\circ$, 14161 measured reflections, 3750 independent reflections ($R_{int}=0.036$), $T=172$ K. The structure was solved by direct methods (SIR97, [47]) and refined by full-matrix least-squares analysis (SHELXL-97). All non-H-atoms were refined anisotropically and H-atoms with isotropic temp. factors. Final agreement factors: $R(gt)=0.0582$, $wR(gt)=0.1706$ for 355 parameters and 2727 observed reflections with $I>2\sigma(I)$. *Cambridge Crystallographic Data Centre* deposition No. CCDC-256500.

Crystallographic data (excluding structure factors) for the structures reported in this paper have been deposited with the *Cambridge Crystallographic Data Centre*. Copies of the data can be obtained, free of charge, on application to the *CCDC,* 12 Union Road, Cambridge CB21EZ UK (fax: +44(1223)336033; e-mail: deposit@ccdc.cam.ac.uk).

REFERENCES

[1] J. M. B. Durand, B. Dagberg, B. E. Uhlin, G. R. Björk, *Mol. Microbiol.* **2000**, *35*, 924.
[2] E. A. Meyer, R. Brenk, R. K. Castellano, M. Furler, G. Klebe, F. Diederich, *ChemBioChem* **2002**, *3*, 250.
[3] R. Brenk, E. A. Meyer, K. Reuter, M. T. Stubbs, G. A. Garcia, F. Diederich, G. Klebe, *J. Mol. Biol.* **2004**, *338*, 55.
[4] E. A. Meyer, M. Furler, F. Diederich, R. Brenk, G. Klebe, *Helv. Chim. Acta* **2004**, *87*, 1333.
[5] C. Romier, R. Ficner, D. Suck, 'Structural Basis of Base Exchange by tRNA-Guanine Transglycosylase', in 'Modification and Editing of RNA', Eds. H. Grosjean, R. Benne, ASM Press, Washington, 1998.
[6] D. M. Goodenough-Lashua, G. A. Garcia, *Bioorg. Chem.* **2003**, *31*, 331.
[7] B. Stengl, K. Reuter, G. Klebe, *ChemBioChem* **2005**, *6*, 1926.
[8] W. Xie, X. Liu, R. H. Huang, *Nat. Struct. Biol.* **2003**, *10*, 781.
[9] D. Iwata-Reuyl, *Bioorg. Chem.* **2003**, *31*, 24.

[10] P. A. Limbach, P. F. Crain, J. A. McCloskey, *Nucleic Acids Res.* **1994**, *22*, 2183.
[11] G. R. Björk, 'Biosynthesis and Function of Modified Nucleosides', in 'tRNA: Structure, Biosynthesis, and Function', Eds. D. Söll, U. L. RajBhandary, ASM Press, Washington, DC, 1995.
[12] G. Dirheimer, W. Baranowski, G. Keith, *Biochimie* **1995**, *77*, 99.
[13] U. Grädler, H.-D. Gerber, D. M. Goodenough-Lashua, G. A. Garcia, R. Ficner, K. Reuter, M. T. Stubbs, G. Klebe, *J. Mol. Biol.* **2001**, *306*, 455.
[14] P. R. Gerber, K. Müller, *J. Comput.-Aided Mol. Design* **1995**, *9*, 251.
[15] G. E. Keyser, N. J. Leonard, *J. Org. Chem.* **1976**, *41*, 3529.
[16] N. J. Leonard, S. P. Hiremath, *Tetrahedron* **1986**, *42*, 1917.
[17] J. Zhang, V. Nair, *Nucleosides Nucleotides* **1997**, *16*, 1091.
[18] H. Liu, J. Gao, S. R. Lynch, Y. D. Saito, L. Maynar, E. T. Kool, *Science* **2003**, *302*, 868.
[19] B. D. Hosangadi, R. H. Dave, *Tetrahedron Lett.* **1996**, *37*, 6375.
[20] K. Sonogashira, Y. Tohda, N. A. Hagihara, *Tetrahedron Lett.* **1975**, *50*, 4467.
[21] P. Pospisil, P. Ballmer, L. Scapozza, G. Folkers, *J. Recept. Signal Transduction* **2003**, *23*, 361.
[22] J. Leszczynski, 'Tautomeric Properties of Nucleic Acid Bases: *Ab Initio* Study', in 'Encyclopedia of Computational Chemistry', John Wiley, Chichester, 1998.
[23] M. Mons, I. Dimicoli, F. Piuzzi, B. Tardivel, M. Elhanine, *J. Phys. Chem. A* **2002**, *106*, 5088.
[24] M. Hanus, F. Ryjacek, M. Kabelac, T. Kubar, T. V. Bogdan, S. A. Trygubenko, P. Hobza, *J. Am. Chem. Soc.* **2003**, *125*, 7678.
[25] J. D. Watson, F. H. C. Crick, *Nature* **1953**, *171*, 964.
[26] X. Yan, T. Hollis, A. F. Monzingo, E. Schelp, J. D. Robertus, G. W. A Milne, S. Wang, *Proteins: Struct., Funct., Genet.* **1998**, *31*, 33.
[27] N. Miyaura, A. Suzuki, *Chem. Rev.* **1995**, *95*, 2457.
[28] E. A. Meyer, R. K. Castellano, F. Diederich, *Angew. Chem.* **2003**, *115*, 1244.
[29] A. Mavridis, I. Moustakali-Mavridis, *Acta Crystallogr., Sect. B* **1977**, *33*, 3612.
[30] S. L. McGovern, E. Caselli, N. Grigorieff, B. K. Shoichet, *J. Med. Chem.* **2002**, *45*, 1712.
[31] A. J. Ryan, N. M. Gray, P. N. Lowe, C. Chung, *J. Med. Chem.* **2003**, *46*, 3448.
[32] K. Reuter, R. Ficner, *J. Bacteriol.* **1995**, *177*, 5284.
[33] R. Brenk, M. T. Stubbs, A. Heine, K. Reuter, G. Klebe, *ChemBioChem* **2003**, *4*, 1066.
[34] S. T. Nonekowski, G. A. Garcia, *RNA* **2001**, *7*, 1432.
[35] F.-L. Kung, G. A. Garcia, *FEBS Lett.* **1998**, *431*, 427.
[36] I. H. Segel, 'Enzyme Kinetics Behavior and Analysis of Rapid Equilibrium and Steady-State Enzyme Systems', John Wiley & Sons, New York, 1993.
[37] H. Bisswanger, 'Enzymkinetik, Theorie und Methoden', Wiley-VCH, Weinheim, **2000**.
[38] R. Brenk, L. Naerum, U. Grädler, H.-D. Gerber, G. A. Garcia, K. Reuter, M. T. Stubbs, G. Klebe, *J. Med. Chem.* **2003**, *46*, 1133.
[39] B. Stengl, R. Brenk, K. Reuter, E. A. Meyer, F. Diederich, G. Klebe, in preparation.
[40] F. Hof, F. Diederich, *Chem. Commun.* **2004**, 477.
[41] M. Kuhn, R. Mecke, *Chem. Ber.* **1961**, *94*, 3016.
[42] ACD/NAME, V. 6.00, Advanced Chemistry Development Inc., Toronto, 2002.
[43] K. Reuter, S. Chong, F. Ullrich, H. Kersten, G. A. Garcia, *Biochemistry* **1994**, *33*, 7041.
[44] GraFit, V. 4.09., *Erithacus Software Ltd*., 1999.
[45] N. J. Leonard, F. Kazmierczak, *J. Org. Chem.* **1987**, *52*, 2933.
[46] Z. Otwinoski, W. Minor, in 'Methods in Enzymology', Eds. C. W. Carter Jr., R. M. Sweet, Academic Press, New York, 1997, p. 307–326.
[47] A. Altomare, M. C. Burla, M. Camalli, G. L. Cascarano, *J. Appl. Crystallogr.* **1999**, *32*, 115.
[48] G. M. Sheldrick, SHELXL-97, Program for the Refinement of Crystal Structures, University of Göttingen, Göttingen, 1997.

Received November 10, 2005